SWIPT Massive MIMO Systems With Active Eavesdropping

Mahmoud Alageli, Aissa Ikhlef, *Senior Member, IEEE*, and Jonathon Chambers, *Fellow, IEEE*

***Abstract*— We consider the optimization of the downlink transmission for simultaneous wireless information and power transfer (SWIPT) in multi-cell massive multiple-input multiple-output systems. The system comprises a two-antenna active energy harvester (EH) which is capable of legitimately harvesting energy via one antenna, and illegitimately and actively eavesdropping the signal intended for certain information user(s) (IU(s)) via the other antenna for the purpose of information decoding or energy harvesting. Thereby, the considered problems are: 1) when the EH eavesdrops for the purpose of information decoding, i.e., the EH is information-untrusted by the base station (BS), we propose to maximize the worst-case secrecy rate under a constraint on a worst-case average harvested energy (AHE) and 2) when the EH eavesdrops one or multiple IUs for energy harvesting, i.e., the EH is information-trusted by the BS, we propose to maximize the sum-rate of the IUs under a constraint on a worst-case AHE by the EH. We derive asymptotic expressions for a lower bound on ergodic secrecy rate (ESR) and AHE in large system limit. Subsequently, we use these results to optimize the power allocation for downlink SWIPT transmissions which include information signals, artificial noise (AN) and energy signal towards the IUs, and legitimate and illegitimate antennas of the EH, respectively. Simulation results show the accuracy of our asymptotic analysis. We show that there is a performance trade-off between the worst-case ESR and the worst-case AHE. In addition, the impact of the combined legitimate/illegitimate operation of the EH on the SWIPT performance is evaluated.**

***Index Terms*— SWIPT, massive MIMO, active eavesdropping, legitimate and illegitimate energy harvesting, physical-layer security, secrecy rate, beamforming, artificial noise.**

I. Introduction

IN THE last few years, with the emerging standardizations of the Internet of Things (IoT), far-field wireless power transfer (WPT) has been of significant importance as a source of energy for remote energy constrained wireless devices such as those related to IoT technologies and wireless sensor networks (WSNs). Far-field WPT in multi-user systems always introduces information security problems as a result of the nature of the broadcast channel. An example of such systems is referred to in the literature as simultaneous wireless information and power transfer (SWIPT) systems in which the transmitter (base station (BS)) supports multiple energy harvesting users (EHs) and multiple information users (IUs). Such systems are expected to show degraded secrecy performance particularly when the EHs actively attack the channel estimation phase for the purpose of information decoding. One of the active eavesdropping attacks is known as the pilot spoofing attack [1], in which during the uplink channel estimation, the eavesdropper (EV) transmits a copy of the training sequence of a certain IU such that the BS estimates the uplink composite channel coefficients of the IU-EV pair of users, and consequently part of the downlink signal intended for the IU will be directed (via downlink beamforming) toward the EV. A pilot spoofing attack is similar to pilot contamination in multi-cell massive multiple-input multiple-output (MIMO) systems [2] except that in the spoofing attack the EV can intentionally control its received leakage information power by controlling its active training power.

Throughout the literature, to the best of the authors' knowledge, the optimized transmission for a SWIPT system with pilot spoofing attack has not been considered. However, there has been research that explores new signal processing methods to enhance the information-secrecy in the presence of a pilot spoofing attack [1], [3]–[9]. The recently developed signal processing algorithms consider recovering network security either by: 1) improving the processing of the signal (which might include the information and/or artificial noise (AN)) transmission [1], [3]–[7]; 2) or by improving both the processing of the signal and the training sequence transmission [8], [9]. The work in [8] considered a MISO setup with an IU-(active EV) pair. Secure transmission is achieved via a two-way training-based scheme in which the transmitter estimates both the IU and the EV channels, then feeds forward the IU with its uplink channel estimate followed by the downlink training sequence. Therefore, the IU can calculate another estimate of its own channel, which will be fed back to the transmitter. Based on the channel estimates available, the transmitter can obtain a better channel estimate by using the uplink and the feedback estimates. This was exploited to improve the optimized downlink beamforming with a secrecy rate objective. The same system setup was considered in [3],

Manuscript received March 19, 2018; revised July 06, 2018; accepted September 06, 2018. Date of publication September 27, 2018; date of current version December 14, 2018. This work was supported by the Engineering and Physical Sciences Research Council (EPSRC), U.K., under Grant EP/R006377/1. *(Corresponding author: Jonathon Chambers.)*

M. Alageli is with the Intelligent Sensing and Communications Group, Newcastle University, Newcastle upon Tyne NE1 7RU, U.K. (e-mail: m.m.a.alageli1@ncl.ac.uk).

A. Ikhlef is with the Department of Engineering, Durham University, Durham DH1 3LE, U.K. (e-mail: aissa.ikhlef@durham.ac.uk).

J. Chambers is with the Intelligent Sensing and Communications Group, Newcastle University, Newcastle upon Tyne NE1 7RU, U.K., also with the College of Automation, Harbin Engineering University, Harbin 150001, China, and also with the University of Leicester, Leicester LE1 7RH, U.K. (e-mail: Jonathon.chambers@le.ac.uk).

Color versions of one or more of the figures in this paper are available online at http://ieeexplore.ieee.org.

Digital Object Identifier 10.1109/JSAC.2018.2872370

however, the EV can decode the information signal and jam the IU in full-duplex mode using two different antenna subsets. In the same way, the transmitter tackles that by jamming the EV using a subset of its antennas, while the remaining antennas are used for information signal transmission. The optimal ratio of transmit/receive antennas was derived to maximize the achievable secrecy degrees of freedom.

WPT and SWIPT with passive EV(s) have been considered for massive MISO/MIMO systems [10]–[17]. The work in [12] considered SWIPT with no secrecy aspect for a massive MIMO system. The harvested energy of the IUs will be used next for uplink training and decoding information simultaneously via splitting the received power. The considered problem was to jointly optimize two sets of variables, power-splitting ratios and the power allocation per IU, to maximize the minimum achievable rate of all the IUs. The variables were optimized alternately. Zhu *et al.* [15] studied the effect of phase noise (at the BS and user antennas) on the IU's information rate and EH's harvested energy in a massive MIMO system and showed that the secrecy rate decreases as phase noise variance increases, while the harvested energy by the EH is not affected. WPT has been considered in [16]–[18]. Kashyap *et al.* [18] demonstrated the impact of having a large transmit antenna array on the harvested energy by a single antenna EH. For matched filter (MF) transmit beamforming, it was proven that any loss in the harvested energy at the EH due to the decrease in the downlink transmit power can be compensated by increasing the number of transmit antennas.

We consider in this paper SWIPT for massive multi-cell MIMO system that comprises multiple single antenna IUs and dual antennas EH which can act as legitimate and active-illegitimate. The EH (located at the reference cell) uses one of its antennas (legitimate antenna) to harvest energy legitimately, while the other antenna (eavesdropping antenna) is used to eavesdrop the information signal of one or multiple IUs. This requires that the EH splits its available channel estimation training power between its own orthogonal training sequence sent from the legitimate antenna, and a copy of the training sequence(s) of the attacked IU(s) sent from the eavesdropping antenna. Therefore, the estimated channel of the attacked IU(s) will be correlated with the eavesdropping antenna channel, consequently, this will strengthen the received information signal power by the active-illegitimate EH.

The main contributions of our work are as follows: 1) We provide closed form expressions (in terms of statistical channel state information (SCSI)) for ESR and average harvested energy (AHE) in large system limit. Such asymptotic analysis is challenging, particularly for a system suffering from instantaneous dependencies between the user's channel vectors and the beamforming vectors in one cell and across different cells due to pilot contamination and active eavesdropping; 2) To tackle the excessive active eavesdropping, unlike conventional AN beamforming [4], [19], we introduce a new design of AN signal such that its jamming effect is directly proportional to the training power invested by the illegitimate active EH, i.e., the larger the eavesdropping training power, the larger the jamming received power at the eavesdropping antenna of the EH; 3) We design an algorithm to optimize the downlink power allocation among the information, AN and energy transmit signal vectors toward the IUs, legitimate and eavesdropping antenna of the EH, respectively. For the information-untrusted EH case, the power allocation aims to maximize the worst-case ESR under a constraint on the worst-case AHE by the EH, while for the information-trusted EH, the considered problem is to maximize the IUs' ergodic sum-rate under a constraint on a worst-case AHE; 4) More importantly, we introduce a new concept of illegitimate energy harvesting which is based on active eavesdropping for the purpose of energy harvesting. The illegitimate EH can maximize its harvested energy by optimally splitting its training power between its own legitimate training sequence and other IUs' training sequences; 5) We provide complexity analysis of the proposed algorithms.

Related Work: The concept of secure SWIPT has been studied for conventional MIMO/MISO systems in [20]–[23]. Liu *et al.* [22] proposed AN-aided SWIPT in a MISO system comprising a single IU and multiple untrusted EHs. The considered problem was the maximization of the worst-case secrecy rate of the IU while maintaining a minimum level of individual harvested energy by each EH. The design in [22] was extended in [23] to consider sum secrecy rate maximization for multiple IUs. Latterly, the secure SWIPT design was extended to massive MIMO systems in [13]–[15]. Wang *et al.* [13] considered secrecy and energy efficiencies in massive MIMO enabled heterogeneous cloud radio access network (C-RAN). The power gain of the channels from the remote radio heads (RRHs) to the IU and the passive EV are known. The contribution of [14] was to optimize the downlink transmission covariance matrix of the IU in a wire-tap massive MIMO system. The ergodic secrecy rate of the IU under a constraint on the harvested energy by the passive EH was considered. Zhu *et al.* [15] studied the secrecy performance of SWIPT massive MIMO system when the uplink training is affected by phase noise. The secure SWIPT in the previous works assumed no active eavesdropping. To the best of the authors' knowledge, optimizing the downlink transmission in an actively wire-taped massive MIMO system has not been studied before. In particular, we assume that the EH employs two antennas, the first antenna is used to illegitimately eavesdrop information signal, while the second antenna is used to legitimately harvest energy. The EH can control splitting the transmit training power between the legitimate and illegitimate antennas.

The remainder of this paper is organized as follows. Section II presents the system model including the channel estimation, downlink transmission and the derivation of the worst-case ESR. Section III provides some random matrix theory results and the large system analysis for the worst-case ESR and the AHE. In Section IV, we present the power allocation optimization for both information-untrusted and information-trusted EH cases. In Section V, we provide the complexity analysis of the proposed algorithms. Simulation results and evaluations are given in Section VI. Finally, we conclude the paper in Section VII.

Notation: Vectors are denoted by boldface lower case letters and matrices by boldface upper case letters. $\boldsymbol{I}_N$, $\mathbf{1}_M$ and

$\mathbf{0}_{m\times n}$ denote the $N\times N$ identity matrix, $M\times 1$ vector with all entries one and the $m\times n$ zero matrix, respectively. diag($\boldsymbol{S}$) is a column vector whose entries are the diagonal entries of matrix $\boldsymbol{S}$. $\boldsymbol{S}\succ 0$ indicates that $\boldsymbol{S}$ is a positive definite matrix. $\rho(\boldsymbol{S})$ gives the largest eigenvalue of matrix $\boldsymbol{S}$. The operators $(\cdot)^T$, $(\cdot)^H$, tr$(\cdot)$, $\log_2(\cdot)$, $|\cdot|$ and $\|\cdot\|$ denote the transpose, conjugate transpose, trace of a matrix, logarithm to base 2, the absolute value of scalars and the Euclidean norm, respectively. $\|[x_1,\ldots,x_M]\|_1=\sum_{i=1}^{M}|x_i|$. $\mathbb{C}^{m\times n}$ denotes the set of all complex $m\times n$ matrices. $\boldsymbol{x}\sim\mathcal{CN}(\mathbf{0},\boldsymbol{\Sigma})$ denotes a circularly symmetric complex Gaussian random vector $\boldsymbol{x}\in\mathbb{C}^{N\times 1}$ with zero mean and covariance matrix $\boldsymbol{\Sigma}$. cov(x,y) and var(x) denote the covariance between the random variables x and y, and the variance of x, respectively. $\{\boldsymbol{a}_n\}$ denotes a set of all vectors indexed by n. $\{a_{m,n}\}_m$ denotes a set of all scalars indexed by m. $[f(N)]_{N\to\infty}=a$ and $f(N)\overset{N\to\infty}{\to}a$ are equivalent to $\lim_{N\to\infty}f(N)=a$ and can be used interchangeably. $[x]^+=\max(x,0)$.

II. System Model

We consider the downlink of a multi-cell massive MIMO system with a cell cluster of size L. Each cell consists of a BS equipped with a large number of antennas N of order of hundreds, M single antenna IUs interested in information decoding, $\{\text{IU}_{l,i}\}$, $i=1,2,\ldots,M$, where $l\in\{1,\ldots,L\}$ is the cell index. We assume that an active EH, equipped with two antennas is located in the reference cell (indexed $l=1$), where one antenna is used to harvest energy legitimately, while the other antenna is used for one of the following two purposes: 1) to illegitimately and actively eavesdrop and decode the information signal intended for a certain IU, $\text{IU}_{1,i}$, $i\in\{1,2,\ldots,M\}$, and in this case the EH is considered as information-untrusted by the BS; 2) to illegitimately and actively harvest energy from the information signal intended for one or multiple IUs, and in this case the EH is considered as information-trusted by the BS. For a massive MIMO system, the assumption of single-antenna IU is reasonable since the large dimensionality of transmit antennas can provide a favorable propagation channel and the required diversity gain at a simple, cheap, single-antenna IU's device [24]. In addition, the favorable propagation channels can perfectly eliminate inter-user interference, therefore, the achievable capacity by M single antenna IUs is equivalent to that of one M-antenna IU [24]. The design of illegitimate spy devices (such as our considered EH) does not have to be subject to accepted standards and such devices can have an exceptional design to ultimately achieve their desired goals. Such exceptional designs for spy and malicious attack devices have been widely adopted in the literature [3].

During the uplink training phase, the EH transmits a copy of the training sequence(s) of the IU(s) under attack, $\{\text{IU}_{1,m}\}$, $\{m\}=\mathcal{M}\subseteq\{1,\ \ldots,M\}$, via its eavesdropping antenna such that the BS estimates the uplink composite channel coefficients — which are equivalent to the downlink channel coefficients based on channel reciprocity in the time division duplexing mode, TDD — of both $\{\text{IU}_{1,m}\}$ channel(s) and the eavesdropping antenna channel of the EH. Consequently, part of the downlink signal intended for the $\text{IU}_{1,i}$ will be directed (beamformed) toward the EH.

Let $\boldsymbol{h}_{i,l,p}=\boldsymbol{R}_{i,l,p}^{\frac{1}{2}}\tilde{\boldsymbol{h}}_{i,l,p}$ denote the uplink channel vector between the ith IU in the lth cell, $\text{IU}_{l,i}$, and the pth cell's BS where $\tilde{\boldsymbol{h}}_{i,l,p}\sim\mathcal{CN}(\mathbf{0},\boldsymbol{I}_N)$ and $\boldsymbol{R}_{i,l,p}\succ 0$ is a Hermitian Toeplitz matrix representing the spatial correlation between the entries of $\boldsymbol{h}_{i,l,p}$. $\boldsymbol{g}_{E_p}=\boldsymbol{R}_{1,p}^{\frac{1}{2}}\tilde{\boldsymbol{g}}_{E_p}$ denotes the uplink channel vector between eavesdropping (illegitimate) antenna of the EH and the pth cell's BS, $\tilde{\boldsymbol{g}}_{E_p}\sim\mathcal{CN}(\mathbf{0},\boldsymbol{I}_N)$ and $\boldsymbol{R}_{1,p}\succ 0$ denotes the spatial correlation between the entries of $\boldsymbol{g}_{E_p}$. $\boldsymbol{g}_p=\boldsymbol{R}_{1,p}^{\frac{1}{2}}\tilde{\boldsymbol{g}}_p$ denotes the uplink channel vector between the legitimate antenna of the EH and the pth cell's BS,[1] $\tilde{\boldsymbol{g}}_p\sim\mathcal{CN}(\mathbf{0},\boldsymbol{I}_N)$.

The variations of the entries of $\tilde{\boldsymbol{h}}_{i,l,p}$, $\tilde{\boldsymbol{g}}_{E_p}$ and $\tilde{\boldsymbol{g}}_p$ give a measure of small-fading coefficients, while path loss and correlation between BS antenna elements are captured by $\boldsymbol{R}_{i,l,p}$ and $\boldsymbol{R}_{l,p}$. We assume that the variance of the channel coefficient between the user and any of its local BS antennas is γ_1, and $\gamma_2<\gamma_1$ to any of the neighbouring BS antennas. Therefore, with the assumption that the EH and the IUs experience statistically equal path loss, the scaling of the correlation matrices satisfies

$$\text{diag}\left(\boldsymbol{R}_{i,l,p}\right),\ \text{diag}\left(\boldsymbol{R}_{l,p}\right)=\begin{cases}\gamma_1\mathbf{1}_N, & l=p\\ \gamma_2\mathbf{1}_N, & l\neq p.\end{cases}\tag{1}$$

A. Uplink Channel Estimation Under Active Attack

The user channels exhibit block fading, i.e., the channels remain constant over a time block and change independently from one block to another. Over each block, the transmission occurs across two time slots for uplink training sequence transmission and downlink signal transmission. The relative division between the two time slots is not considered in this paper, however, we assume a unit time slot for downlink transmission as in [14] and [22]. During the uplink training phase, a pilot training is sent from each IU, $\{\text{IU}_{l,i}\}$, with an average power P_I. The EH sends a copy of training sequence(s) of the attacked IU(s) via its eavesdropping antenna using part of its total average power ϕP_E, $0<\phi<1$, while the remaining training power $(1-\phi)P_E$ is used for transmitting the legitimate energy harvesting training sequence via the second antenna. The training sequences of the IUs and legitimate EH in a single cell are assumed to be orthogonal, but since the channel coherence time is limited, the training sequences are reused across all cells.

The signal at the pth BS received across τ training transmissions is

$$\boldsymbol{Y}_p=\sum_{l=1}^{L}\sum_{i=1}^{M}\sqrt{P_I}\boldsymbol{h}_{i,l,p}\boldsymbol{\psi}_i^T+(1-\phi)P_E\boldsymbol{g}_p\boldsymbol{\psi}_E^T+\sum_{j\in\mathcal{M}}\sqrt{\frac{\phi P_E}{|\mathcal{M}|}}\,\boldsymbol{g}_{E_p}\boldsymbol{\psi}_j^T+\boldsymbol{N}_p,\tag{2}$$

[1]Since the separation between the legitimate and illegitimate antennas of the EH is much smaller than the distance from the EH to the BS's antenna array and local scatterers, the angles of arrivals of the signals from both antennas at the BS's antenna array are identical. This implies that the channel vectors $\boldsymbol{g}_p$ and $\boldsymbol{g}_{E,p}$ experience the same spatial correlation between their entries [25], [26].

where $\boldsymbol{N}_p \in \mathbb{C}^{N\times\tau}$ is the additive noise matrix with entries following the distribution $\mathcal{CN}(0,\sigma_n^2)$. $\mathcal{M}$ is the set of IUs eavesdropped by the EH and $|\mathcal{M}|$ is the cardinality of $\mathcal{M}$. $\boldsymbol{\psi}_i \in \mathbb{C}^{\tau\times 1}$ and $\boldsymbol{\psi}_E \in \mathbb{C}^{\tau\times 1}$ are the training sequences of $\text{IU}_{l,i}$, $\forall l$, and the legitimate antenna of the EH, respectively. $\boldsymbol{\psi}_i^H\boldsymbol{\psi}_{j\neq i}$, $\boldsymbol{\psi}_i^H\boldsymbol{\psi}_E = 0$; and $\boldsymbol{\psi}_i^H\boldsymbol{\psi}_i$, $\boldsymbol{\psi}_E^H\boldsymbol{\psi}_E = \tau$. The minimum mean square error (MMSE) estimate of $\boldsymbol{h}_{i,p,p}$, $\hat{\boldsymbol{h}}_{i,p,p}$ is given as

$$\hat{\boldsymbol{h}}_{i,p,p} = \boldsymbol{C}_{p,i}\,\boldsymbol{y}_{p,i}, \tag{3a}$$

$$\boldsymbol{y}_{p,i} = \tau\sqrt{P_I}\sum_{l=1}^{L}\boldsymbol{h}_{i,l,p} + \alpha\tau\sqrt{\frac{\phi P_E}{|\mathcal{M}|}}\,\boldsymbol{g}_{E_p} + \boldsymbol{N}_p\boldsymbol{\psi}_{I_i}^*, \tag{3b}$$

$$\boldsymbol{C}_{p,i} = \sqrt{P_I}\boldsymbol{R}_{i,p,p} \times\left(\tau P_I\sum_{l=1}^{L}\boldsymbol{R}_{i,l,p}+\frac{\alpha\tau\phi P_E}{|\mathcal{M}|}\boldsymbol{R}_{1,p}+\sigma_n^2\boldsymbol{I}_N\right)^{-1}, \tag{3c}$$

where $\boldsymbol{y}_{p,i} \in \mathbb{C}^{N\times 1}$ is the projection of $\boldsymbol{Y}_p$ onto $\boldsymbol{\psi}_{I_i}$, $\boldsymbol{C}_{p,i} \in \mathbb{C}^{N\times N}$ is the MMSE estimation matrix, $\alpha = 1$ for $i \in \mathcal{M}$ and $\alpha = 0$ for $i \notin \mathcal{M}$. The covariance matrix of $\hat{\boldsymbol{h}}_{i,p,p}$ is $\hat{\boldsymbol{R}}_{I_{i,p,p}} = E[\hat{\boldsymbol{h}}_{i,p,p}\hat{\boldsymbol{h}}_{i,p,p}^H] = \tau\sqrt{P_I}\boldsymbol{C}_{p,i}\,\boldsymbol{R}_{i,p,p}$. Similarly, for the case of information-untrusted EH in which one IU, $\text{IU}_{1,i}$, is being attacked for information eavesdropping (i.e., $|\mathcal{M}| = 1$), the MMSE estimate of $\boldsymbol{g}_{E_1}$, $\hat{\boldsymbol{g}}_{E_{1,i}}$, is given as

$$\hat{\boldsymbol{g}}_{E_{1,i}} = \boldsymbol{C_i}\,\boldsymbol{y}_{1,i}, \tag{4a}$$

$$\boldsymbol{C_i} = \sqrt{\phi P_E}\boldsymbol{R}_{1,1} \times\left(\tau P_I\sum_{l=1}^{L}\boldsymbol{R}_{i,l,p} + \tau\phi P_E\boldsymbol{R}_{1,1} + \sigma_n^2\boldsymbol{I}_N\right)^{-1}. \tag{4b}$$

The covariance matrix of $\hat{\boldsymbol{g}}_{E_{1,i}}$ is $\hat{\boldsymbol{R}}_i = E[\hat{\boldsymbol{g}}_{E_{1,i}}\hat{\boldsymbol{g}}_{E_{1,i}}^H] = \tau\sqrt{P_E}\boldsymbol{C}_i\,\boldsymbol{R}_{1,1}$. The estimation of $\boldsymbol{g}_p$ is not required since, as we will see later, we use retrodirective beamforming [15]. The MMSE estimation results in (3) and (4) follows from the standard linear estimation theory [27], [28].

Remark 1: We assume that the reference cell's BS blames the information-untrusted EH for the active eavesdropping attack. The BS has the ability to calculate the eavesdropping training power by using the following lemma.

Lemma 1: Having $N \to \infty$, any illegitimate active training power associated with the training sequence $\boldsymbol{\psi}_{I_i}$, can be detected and calculated as

$$\frac{\boldsymbol{y}_{1,i}^H\boldsymbol{y}_{1,i} - \tau^2 P_I\sum_{t=1}^{L}\text{tr}\left(\boldsymbol{R}_{i,t,1}\right) + N\tau\sigma_n^2}{\tau^2\text{tr}\left(\boldsymbol{R}_{1,1}\right)} \overset{N\to\infty}{\to} \begin{cases}\dfrac{\phi P_E}{|\mathcal{M}|}, & i\in\mathcal{M}\\ 0, & i\notin\mathcal{M},\end{cases} \tag{5}$$

where all the scalars, vector and matrices in (5) are deterministic at the BS.

Proof: See Appendix A. ∎

Alternatively, the detection of the active eavesdropper is possible by averaging the difference covariance matrix $\boldsymbol{y}_{1,i}\boldsymbol{y}_{1,i}^H - \bar{\boldsymbol{R}}_i$ over some data blocks, where $\bar{\boldsymbol{R}}_i = \left(\tau^2 P_I\sum_{l=1}^{L}\boldsymbol{R}_{i,l,1} + \tau\sigma_n^2\boldsymbol{I}_N\right)$ and it is deterministic at the BS [4]. In addition, we assume a perfect knowledge of the SCSIs, $\{\boldsymbol{R}_{i,l,1}\}$ and $\boldsymbol{R}_{1,1}$, at the reference cell's BS, which is reasonable, particularly for the massive antenna array at the BS [29].

B. Downlink Transmission

The pth BS employs transmit MF beamforming to direct the information signal vector $\sum_{i=1}^{M}\sqrt{P_{p,i}}\,\boldsymbol{w}_{i,p}\,x_{i,p}$, toward its local IUs, where $P_{p,i}$ is the power allocated to $\text{IU}_{p,i}$ and

$$\boldsymbol{w}_{i,p} = \hat{\boldsymbol{h}}_{i,p,p}^*/\|\hat{\boldsymbol{h}}_{i,p,p}\|, \tag{6}$$

is a unit norm information beamforming vector for $\text{IU}_{p,i}$ and $x_{i,p}$ is the information symbol intended for $\text{IU}_{p,i}$, with $x_{i,p} \sim \mathcal{CN}(0,1)$. The information symbols are assumed to be mutually independent. The reference BS directs the energy signal vector $\boldsymbol{w}$ toward the legitimate antenna of the EH. The energy signal is designed using retrodirective beamforming [17] in which the reference BS retransmits an amplified conjugated version of the received energy training sequence, such that $\boldsymbol{w} = \sqrt{P}\boldsymbol{y}^*/\|\boldsymbol{y}\|$, where

$$\boldsymbol{y} = \boldsymbol{Y}_1\boldsymbol{\psi}_E^* = \tau\sqrt{(1-\phi)P_E}\,\boldsymbol{g}_1 + \boldsymbol{N}_1\boldsymbol{\psi}_E^*. \tag{7}$$

For the information-untrusted EH case, the BS facilitates secure information decoding at the attacked $\text{IU}_{1,i}$ and energy harvesting at the EH simultaneously by directing the AN signal vector $\sqrt{P_n}\boldsymbol{w}_{n_i}z$ toward the EH

$$\boldsymbol{w}_{n_i} = \hat{\boldsymbol{g}}_{E_{1,i}}^*/\|\hat{\boldsymbol{g}}_{E_{1,i}}\|, \tag{8}$$

where $z \sim \mathcal{CN}(0,1)$ is the AN symbol and P_n is the power allocated to $\boldsymbol{w}_{n_i}$. With the new design approach for the AN beamformer in (8), it can be noticed that the received AN signal at the eavesdropping antenna of the EH, $P_n|\boldsymbol{g}_{E_1}^T\hat{\boldsymbol{g}}_{E_{1,i}}^*|^2/\|\hat{\boldsymbol{g}}_{E_{1,i}}\|^2$, is directly proportional to the eavesdropping training power, ϕP_E (since $\hat{\boldsymbol{g}}_{E_{1,i}} \propto \sqrt{\phi P_E}\boldsymbol{g}_{E_1}$). Therefore, $\boldsymbol{w}_{n_i}$ is able to tackle any excessive active eavesdropping, i.e., the larger the eavesdropping training power, the larger the jamming received power by the EH.

Given that $\text{IU}_{1,i}$ is the IU being attacked, then the received signals at $\text{IU}_{1,i}$, y_{I_i}; the legitimate antenna of the EH, y_{1_i}; and at the eavesdropping antenna of the EH, y_{E_i}, are

$$y_{I_i} = \sum_{p=1}^{L}\sum_{j=1}^{M}\sqrt{P_{p,j}}\,\boldsymbol{h}_{i,1,p}^T\,\boldsymbol{w}_{j,p}\,x_{j,p} + \sqrt{P}\;\boldsymbol{h}_{i,1,1}^T\,\boldsymbol{w} + \sqrt{P_n}\;\boldsymbol{h}_{i,1,1}^T\,\boldsymbol{w}_{n_i}z + n_{I_i}, \tag{9}$$

$$y_{1_i} = \sum_{p=1}^{L}\sum_{j=1}^{M}\sqrt{P_{p,j}}\,\boldsymbol{g}_p^T\,\boldsymbol{w}_{j,p}\,x_{j,p} + \sqrt{P}\;\boldsymbol{g}_1^T\,\boldsymbol{w} + \sqrt{P_n}\;\boldsymbol{g}_1^T\,\boldsymbol{w}_{n_i}z + n_1, \tag{10}$$

$$y_{E_i} = \sum_{p=1}^{L}\sum_{j=1}^{M}\sqrt{P_{p,j}}\,\boldsymbol{g}_{E_p}^T\,\boldsymbol{w}_{j,p}\,x_{j,p} + \sqrt{P}\;\boldsymbol{g}_{E_1}^T\,\boldsymbol{w} + \sqrt{P_n}\;\boldsymbol{g}_{E_1}^T\,\boldsymbol{w}_{n_i}z + n_E, \tag{11}$$

where n_{I_i}, n_1 and n_E are zero mean σ_n^2 variance complex Gaussian noises at $\text{IU}_{1,i}$, the legitimate and eavesdropping antennas of the EH, respectively.

C. Achievable Lower Bound on the Information User Ergodic Rate

In massive MIMO systems with pilot contamination and active eavesdropping, since the precoded channel $\boldsymbol{h}_{i,1,1}^T \boldsymbol{w}_{i,1}$ is not known at $\text{IU}_{1,i}$, we apply the method used in [2] and [30] to derive a lower bound on the ergodic rate. In particular, the received information signal at $\text{IU}_{1,i}$ in (9) can be recast as

$$y_{I_i} = \sqrt{P_{1,i}} E[a_{i,i}^{(1)}]\ x_{i,1} + \sqrt{P_{1,i}} \left(a_{i,i}^{(1)} - E[a_{i,i}^{(1)}]\right) x_{i,1} + Z_i, \tag{12}$$

where

$$\begin{aligned} Z_i &= \sum_{j\neq i}^{M} \sqrt{P_{1,j}} a_{i,j}^{(1)} x_{j,1} + \sqrt{P} a_{1_i} + \sqrt{P_n} a_i z + \hat{a}_i + n_{I_i}, \\ a_{i,j}^{(p)} &= \boldsymbol{h}_{i,1,p}^T\, \boldsymbol{w}_{j,p}, \quad \tilde{a}_i = a_{i,i}^{(1)} - E[a_{i,i}^{(1)}],\ a_{1_i} = \boldsymbol{h}_{i,1,1}^T\, \boldsymbol{w}, \\ a_i &= \boldsymbol{h}_{i,1,1}^T\, \boldsymbol{w}_{n_i} \ \text{ and } \ \hat{a}_i = \sum_{p=2}^{L} \sum_{j=1}^{M} \sqrt{P_{p,j}} a_{i,j}^{(p)} x_{j,p}. \end{aligned} \tag{13}$$

$\sqrt{P_{1,i}} E[a_{i,i}^{(1)}] x_{i,1}$ is the desired signal received over the deterministic average precoded channel $E[a_{i,i}^{(1)}]$.[2] $\sqrt{P_{1,i}}\ \tilde{a}_i\ x_{i,1} = \sqrt{P_{1,i}}(a_{i,i}^{(1)} - E[a_{i,i}^{(1)}]) x_{i,1}$ is the beamforming uncertainty, which is the desired signal over unknown channel to the information user. $\sum_{j\neq i}^{M} \sqrt{P_{1,j}} a_{i,j}^{(1)} x_{j,1}$, $\sqrt{P} a_{1_i}$, $\sqrt{P_n} a_i z$ and $\hat{a}_i$ in Z_i are the reference cell inter user interference, energy signal, AN signal and the interference from neighbouring cells at $\text{IU}_{1,i}$, respectively. Now, using [2, Th. 1], we have the following lower bound on ergodic information rate at the attacked IU, $\text{IU}_{1,i}$

$$R_i = \log_2 \left(1 + \text{SINR}_{I_i}\right), \tag{14}$$

where

$$\begin{aligned} \text{SINR}_{I_i} &= \frac{P_{1,i}\ \left| E\left[a_{i,i}^{(1)}\right] \right|^2}{P_{1,i} \text{var}\left[a_{i,i}^{(1)}\right] + E\left[\left|Z_i\right|^2\right]}, \\ \text{var}\left[a_{i,i}^{(1)}\right] &= E\left[\left| a_{i,i}^{(1)} - E\left[a_{i,i}^{(1)}\right]\right|^2\right] = E\left[\left|\tilde{a}_i\right|^2\right]. \end{aligned} \tag{15}$$

D. Upper Bound on the EH Ergodic Rate

The received information signal of $\text{IU}_{1,i}$ at the eavesdropping antenna of the EH in (11) is recast as

$$\begin{aligned} y_{E_i} = \sqrt{P_{1,i}} b_{i,1} x_{i,1} + \sum_{j\neq i}^{M} \sqrt{P_{1,j}} b_{j,1} x_{j,1} + \sqrt{P} b \\ + \sqrt{P_n}\ b_i\ z + \hat{b}_i + n_E, \end{aligned} \tag{16}$$

where

$$\begin{aligned} b_{j,p} &= \boldsymbol{g}_{E_p}^T\, \boldsymbol{w}_{j,p}, \quad b = \boldsymbol{g}_{E_1}^T\, \boldsymbol{w},\ b_i = \boldsymbol{g}_{E_1}^T \boldsymbol{w}_{n_i}, \\ \hat{b}_i &= \sum_{p=2}^{L} \sum_{j=1}^{M} \sqrt{P_{p,j}} b_{j,p} x_{j,p}. \end{aligned} \tag{17}$$

$\sqrt{P_{1,i}} b_{i,1} x_{i,1}$ is the desired received signal. $\sum_{j\neq i}^{M} \sqrt{P_{1,j}}\ b_{j,1} x_{j,1}$, $\sqrt{P} b$, $\sqrt{P_n}\ b_i\ z$ and $\hat{b}_i$ are the reference cell inter user interference, energy signal, AN signal and the interference from neighbouring cells at the eavesdropping antenna of the EH, respectively. In the following, we assume that the EH has full knowledge of the IUs' beamforming vectors $\{\boldsymbol{w}_{j,1}\}$ and its own channels $\{\boldsymbol{g}_{E_1},\ \boldsymbol{g}_1\}$; and is able to cancel the intra-cell interference. This results in an upper bound on the EH ergodic rate. We state the following theorem.

Theorem 1: For $N \to \infty$ and assuming that the EH has full knowledge of the IUs' beamforming vectors and its own channels; and is able to cancel the intra-cell interference, an upper bound on the ergodic rate of the EH is given by

$$R_{E_i} \overset{N\to\infty}{\to} \log_2 \left(1 + \text{SINR}_{E_i}\right), \tag{18}$$

where

$$\text{SINR}_{E_i} = \frac{P_{1,i} E\left[\left|b_{i,1}\right|^2\right]}{P E\left[\left|b\right|^2\right] + P_n E\left[\left|b_i\right|^2\right] + E\left[\left|\hat{b}_i\right|^2\right] + \sigma_n^2}. \tag{19}$$

Proof: See Appendix B. ∎

E. Lower Bound on Ergodic Secrecy Rate

Based on the information rate bounds in (14) and (18), we have the following lower bound of the ESR of the attacked IU, $\text{IU}_{1,i}$

$$R_{S_i} \overset{N\to\infty}{\to} \left[R_i - R_{E_i}\right]^+. \tag{20}$$

It is worth noting that R_{S_i} represents the worst-case scenario for the secrecy performance since we have a lower bound on the IU ergodic rate and an upper bound on the EH ergodic rate. As a result, achieving security for this worst-case scenario implies achieving security for a more optimistic scenario [4], [20].

F. Average Harvested Energy

Given a unit time slot for downlink transmission and an equal energy harvesting efficiency for all users, $0 < \zeta < 1$, the AHE by the EH depends on the attacked IU, $\text{IU}_{1,i}$, and is given as[3]

$$\begin{aligned} E_i = \zeta E\left[\sum_j P_{1,j}\ \left|b_{j,1}\right|^2 + P\left|b\right|^2 + P_n\left|b_i\right|^2 + \left|\hat{b}_i\right|^2\right] \\ + \zeta E\left[\sum_j P_{1,j}\ \left|\tilde{b}_{j,1}\right|^2 + P\left|\tilde{b}\right|^2 + P_n\left|\tilde{b}_i\right|^2 + \left|\ddot{b}_i\right|^2\right], \end{aligned} \tag{21}$$

[2] As $N \to \infty$, $E[a_{i,i}]$ always converges to a positive real deterministic value (see Appendix A).

[3] Since the EH is information-untrusted by the BS, therefore, the energy is considered to be harvested from the energy, AN and information signals. Also considering AHE is reasonable since as $N \to \infty$, the total harvested energy is dominated by its average [10].

where

$$\tilde{b}_{j,p} = \boldsymbol{g}_p^T \boldsymbol{w}_{j,p},\ \tilde{b} = \boldsymbol{g}_1^T \boldsymbol{w},\ \tilde{b}_i = \boldsymbol{g}_1^T \boldsymbol{w}_{n_i},$$
$$\ddot{b}_i = \sum_{p=2}^{L} \sum_{j=1}^{M} \sqrt{P_{p,j}} \tilde{b}_{j,p}. \tag{22}$$

For the case of information-trusted EH, the secrecy issue is not relevant and the design aims to jointly improve both the ergodic sum-rate, $\sum_i R_i$ and the AHE which depends on the set of attacked IUs, $\mathcal{M}$. The expression at the right-hand side of (21) is still valid for calculating the AHE in this case. The optimization of downlink power allocation is left to be considered in section IV. In the next section, we consider the large system analysis.

III. Large System Analysis

In this section, we analyze and derive the asymptotic convergence of the expected values of the received powers of the normalized transmit signals at the IUs and the EH, $E[\{a_{i,i}^{(1)}, |a_{i,j}^{(p)}|^2,\ |\tilde{a}_i|^2,\ |a_{1_i}|^2,\ |a_i|^2,\ |\hat{a}_i|^2\}]$; $E[\{|b_{i,p}|^2,\ |b|^2,\ |b_i|^2,\ |\hat{\tilde{b}}_i|^2\}]$ and $E[\{|\tilde{b}_{j,p}|^2,\ |\tilde{b}|^2,\ |\tilde{b}_i|^2, |\ddot{b}_i|^2\}]$, respectively, with the condition that the number of transmit antennas is very large, i.e., $N \to \infty$. The assumption of $N \to \infty$ is valid and commonly used in the massive MIMO literature. It helps in simplifying the design and analysis of massive MIMO systems. After obtaining the design parameters using this assumption, the system's performance can be tested for the practical case of large but limited number of antennas [3], [12], [17], [19].

A. Random Matrix Theory Preliminaries

Some random matrix theory results are used to calculate the converged expected values of the received signal and interference powers in terms of: correlation matrices $\{\boldsymbol{R}_{1,p}\} = \mathcal{R}_E$ and $\{\boldsymbol{R}_{i,l,p}\} = \mathcal{R}_I$ which include the channel path loss, training powers P_I, ϕP_E and $(1-\phi)P_E$; allocated transmit powers $\{P_{p,j}\}$, P and P_n; and the channel estimation matrices $\{\boldsymbol{C}_{p,i}\} = \mathcal{C}_I$ and $\{\boldsymbol{C}_i\} = \mathcal{C}_E$.

For evaluating the asymptotic values of the received signal and interference powers we use *Corollary 1* in [31] which is quoted as:

Corollary 1: "Let $\boldsymbol{A}$ be a deterministic $N \times N$ complex matrix with uniformity bounded spectral radius for all N. Let $\boldsymbol{q} = \frac{1}{\sqrt{N}}[q_1, \ldots, q_N]$ where the q_i's are i.i.d. complex random variables with zero mean, unit variance, and finite eighth moment. Let $\boldsymbol{r}$ be a similar vector independent of $\boldsymbol{q}$. Then

$$\left[\boldsymbol{q}^H \boldsymbol{A} \boldsymbol{q} - \frac{1}{N}\text{tr}\,(\boldsymbol{A})\right] \to 0 \ \text{ and } \ \left[\boldsymbol{q}^H \boldsymbol{A} \boldsymbol{r}\right] \to 0$$

almost surely as $N \to \infty$."

To make use of the above result, we need to investigate the spectral boundedness of correlation matrices, channel estimation matrices and their product. We have the following lemmas.

Lemma 2: The spectral radii of the correlation matrices $\mathcal{R}_E$ and $\mathcal{R}_I$ are upper bounded as

$$\{\rho(\boldsymbol{R}_{1,p})\} \le \begin{cases} \gamma_1, & p = 1 \\ \gamma_2, & p \ne 1, \end{cases} \quad \{\rho\left(\boldsymbol{R}_{i,l,p}\right)\} \le \begin{cases} \gamma_1, & l = p \\ \gamma_2, & l \ne p. \end{cases} \tag{23}$$

Lemma 3: The spectral radii of the channel estimation matrices $\mathcal{C}_I$ and $\mathcal{C}_E$ are upper bounded as

$$\{\rho(\boldsymbol{C}_{i,p})\},\ \{\rho(\boldsymbol{C}_i)\} \le c \le \infty, \tag{24}$$

where c is a positive real scalar.

Lemma 4: Let a finite set $\{\boldsymbol{A}_m\} \subset \{\mathcal{R}_I, \mathcal{R}_E, \mathcal{C}_I, \mathcal{C}_E\}$ and $\exists \boldsymbol{A}_m \in \{\mathcal{R}_I, \mathcal{R}_E\}$, $\exists \boldsymbol{A}_m \in \{\mathcal{C}_I, \mathcal{C}_E\}$. Then, the spectral radius of $\prod_m \boldsymbol{A}_m$ is always bounded with a definite value, $\rho(\prod_m \boldsymbol{A}_m) < \infty$.

Lemma 5: Having the column vectors $\boldsymbol{x} = [\boldsymbol{\Theta}_1 \boldsymbol{x}_1 + \cdots + \boldsymbol{\Theta}_N \boldsymbol{x}_N]$ and $\boldsymbol{y} = [\bar{\boldsymbol{\Theta}}_1 \boldsymbol{y}_1 + \cdots + \bar{\boldsymbol{\Theta}}_N \boldsymbol{y}_N]$, where $\{\boldsymbol{x}_j\}$ and $\{\boldsymbol{y}_j\}$ are statistically independent and follow the distribution $\mathcal{CN}(\boldsymbol{0}, \boldsymbol{I}_N)$. Then, for an arbitrary matrix $\boldsymbol{A}$ independent of $\{\boldsymbol{x}_j\}$ and $\{\boldsymbol{y}_j\}$ with $\rho(\boldsymbol{A})$, $\rho(\boldsymbol{\Theta}_j)$, $\rho(\bar{\boldsymbol{\Theta}}_j) < \infty$, we have:

$$E\left[\left|\boldsymbol{x}^H \boldsymbol{A} \boldsymbol{y}\right|^2\right] \overset{N\to\infty}{\to} \text{tr}\left(\boldsymbol{A}\, E\left[\boldsymbol{y}\boldsymbol{y}^H\right] E\left[\boldsymbol{x}\boldsymbol{x}^H\right] \boldsymbol{A}^H\right). \tag{25}$$

The proofs of Lemmas 2-5 are provided in Appendix A.

B. Asymptomatic Analysis Results

Using the random matrix theory results in Subsection III-A and given that $\text{IU}_{1,i}$ is the attacked IU, the expected values of the received signal powers at $\text{IU}_{1,i}$, $E[\{a_{i,i}^{(1)}, |a_{i,j}^{(p)}|^2,\ |\tilde{a}_i|^2,\ |a_{1_i}|^2,\ |a_i|^2,\ |\hat{a}_i|^2\}]$, and the expected values of the received signal powers at the EH, $E[\{|b_{i,p}|^2,\ |b|^2,\ |b_i|^2,\ |\hat{b}_i|^2\}]$, asymptomatically converge to definite values as in (27a)–(28e). For notational convenience, we define

$$E\left[\left\{a_{i,i}^{(1)}, \left|a_{i,j}^{(p)}\right|^2,\ |\tilde{a}_i|^2,\ |a_{1_i}|^2,\ |a_i|^2,\ |\hat{a}_i|^2\right\}\right]$$
$$= \left\{\bar{a}_{i,i}^{(1)},\ \bar{a}_{i,j}^{(p)},\ \bar{\tilde{a}}_i,\ \bar{a}_{1_i},\ \bar{a}_i,\ \bar{\hat{a}}_i\right\} \text{ and}$$
$$E\left[\left\{|b_{i,p}|^2,\ |b|^2,\ |b_i|^2,\ \left|\hat{b}_i\right|^2\right\}\right] = \left\{\bar{b}_{i,p},\ \bar{b},\ \bar{b}_i,\ \bar{\hat{b}}_i\right\}. \tag{26}$$

The detailed derivations of the asymptomatic analysis results in (27a)–(28e) are provided in Appendix C.

$$\bar{a}_{i,i}^{(1)} \overset{N\to\infty}{\to} \tau\sqrt{P_I}\,\text{tr}\left(\boldsymbol{\Gamma}_{i,1}\right) \text{tr}^{-\frac{1}{2}}\left(\hat{\boldsymbol{R}}_{i,1,1}\right), \tag{27a}$$
$$\bar{a}_{i,i}^{(p\ne 1)} \overset{N\to\infty}{\to} \left[\tau^2 P_I \left|\text{tr}\left(\boldsymbol{\Gamma}_{i,p}\right)\right|^2 + \text{tr}\left(\boldsymbol{R}_{i,1,p}\tilde{\boldsymbol{R}}_{i,p,p}^{(1)}\right)\right] \times \text{tr}^{-1}\left(\hat{\boldsymbol{R}}_{i,p,p}\right), \tag{27b}$$
$$\bar{a}_{i,j\ne i}^{(p)} \overset{N\to\infty}{\to} \text{tr}\left(\boldsymbol{R}_{i,1,p}\hat{\boldsymbol{R}}_{j,p,p}\right) \text{tr}^{-1}\left(\hat{\boldsymbol{R}}_{j,p,p}\right), \tag{27c}$$
$$\bar{\tilde{a}}_i \overset{N\to\infty}{\to} \text{tr}\left(\boldsymbol{R}_{i,1,1}\,\tilde{\boldsymbol{R}}_{i,1,1}^{(1)}\right) \text{tr}^{-1}\left(\hat{\boldsymbol{R}}_{i,1,1}\right), \tag{27d}$$
$$\bar{a}_{1_i} \overset{N\to\infty}{\to} \text{tr}\left(\boldsymbol{R}_{i,1,1}\,\boldsymbol{\Omega}\right) \text{tr}^{-1}\left(\boldsymbol{\Omega}\right), \tag{27e}$$
$$\bar{a}_i \overset{N\to\infty}{\to} \left[\tau^2 P_I \left|\text{tr}\left(\boldsymbol{\Omega}_i\right)\right|^2 + \text{tr}\left(\boldsymbol{R}_{i,1,1}\tilde{\boldsymbol{R}}_i^{(1)}\right)\right] \text{tr}^{-1}\left(\hat{\boldsymbol{R}}_i\right), \tag{27f}$$

$$\bar{\hat{a}}_i \overset{N\to\infty}{\to} \sum_{p=2}^{L}\sum_{j=1}^{M} P_{p,j}\bar{a}_{i,j}^{(p)}. \tag{27g}$$

$$\bar{b}_{i,p} \overset{N\to\infty}{\to} \left[\tau^2\phi P_E \left|\text{tr}\left(\bar{\boldsymbol{\Gamma}}_{i,p}\right)\right|^2 + \text{tr}\left(\boldsymbol{R}_{1,p}\tilde{\boldsymbol{R}}_{i,p,p}^{(2)}\right)\right] \times \text{tr}^{-1}\left(\hat{\boldsymbol{R}}_{i,p,p}\right), \tag{28a}$$

$$\bar{b}_{j\neq i,p} \overset{N\to\infty}{\to} \text{tr}\left(\boldsymbol{R}_{1,p}\,\hat{\boldsymbol{R}}_{j,p,p}\right)\text{tr}^{-1}\left(\hat{\boldsymbol{R}}_{j,p,p}\right), \tag{28b}$$

$$\bar{b} \overset{N\to\infty}{\to} \text{tr}\left(\boldsymbol{R}_{1,1}\,\boldsymbol{\Omega}\right)\text{tr}^{-1}\left(\boldsymbol{\Omega}\right), \tag{28c}$$

$$\bar{b}_i \overset{N\to\infty}{\to} \left[\tau^2\phi P_E \left|\text{tr}\left(\bar{\boldsymbol{\Omega}}_i\right)\right|^2 + \text{tr}\left(\boldsymbol{R}_{1,1}\tilde{\boldsymbol{R}}_i^{(2)}\right)\right] \times \text{tr}^{-1}\left(\hat{\boldsymbol{R}}_i\right), \tag{28d}$$

$$\bar{\hat{b}}_i \overset{N\to\infty}{\to} \sum_{p=2}^{L}\sum_{j=1}^{M} P_{p,j}\; b''_{j,p}, \tag{28e}$$

where

$$\begin{aligned}
&\boldsymbol{\Gamma}_{i,p} = \boldsymbol{R}_{i,1,p}\boldsymbol{C}_{p,i},\ \tilde{\boldsymbol{R}}_{i,p,p}^{(1)} = \hat{\boldsymbol{R}}_{i,p,p} - \tau^2 P_I \boldsymbol{C}_{p,i}\boldsymbol{R}_{i,1,p}\boldsymbol{C}_{p,i}^H,\\
&\boldsymbol{\Omega} = \tau^2(1-\phi)P_E\boldsymbol{R}_{1,1} + \tau\sigma_n^2\boldsymbol{I}_N,\\
&\boldsymbol{\Omega}_i = \boldsymbol{R}_{i,1,1}\boldsymbol{C}_i,\ \tilde{\boldsymbol{R}}_i^{(1)} = \hat{\boldsymbol{R}}_i - \tau^2 P_I \boldsymbol{C}_i\boldsymbol{R}_{i,1,1}\boldsymbol{C}_i^H,\\
&\bar{\boldsymbol{\Gamma}}_{i,p} = \boldsymbol{R}_{1,p}\boldsymbol{C}_{p,i},\ \tilde{\boldsymbol{R}}_{i,p,p}^{(2)} = \hat{\boldsymbol{R}}_{i,p,p} - \tau^2\phi P_E \boldsymbol{C}_{p,i}\boldsymbol{R}_{1,p}\boldsymbol{C}_{p,i}^H,\\
&\bar{\boldsymbol{\Omega}}_i = \boldsymbol{R}_{1,1}\boldsymbol{C}_i,\ \tilde{\boldsymbol{R}}_i^{(2)} = \hat{\boldsymbol{R}}_i - \tau^2\phi P_E \boldsymbol{C}_i\boldsymbol{R}_{1,1}\boldsymbol{C}_i^H.
\end{aligned} \tag{29}$$

The expected values of the average received powers of the normalized transmit signals at the legitimate antenna of the EH when attacking $\text{IU}_{1,i}$ (in (22)) asymptomatically converge to definite values as in (30). For notational convenience, we define $E[\{|\tilde{b}_{j,p}|^2,\ |\tilde{b}|^2,\ |\dot{b}_i|^2,\ |\dot{b}_i|^2\}] = \{\bar{\tilde{b}}_{j,p},\ \bar{\tilde{b}},\ \bar{\dot{b}}_i,\ \bar{\ddot{b}}_i\}$. The detailed derivations of these asymptomatic values are in Appendix C.

$$\bar{\tilde{b}}_{j,p} \overset{N\to\infty}{\to} \text{tr}\left(\boldsymbol{R}_{1,p}\hat{\boldsymbol{R}}_{j,p,p}\right)\text{tr}^{-1}\left(\hat{\boldsymbol{R}}_{j,p,p}\right), \tag{30a}$$

$$\bar{\tilde{b}} \overset{N\to\infty}{\to} \left[\tau^2(1-\phi)P_E\text{tr}^2\left(\boldsymbol{R}_{1,1}\right) + \tau\sigma_n^2\text{tr}\left(\boldsymbol{R}_{1,1}\right)\right]\text{tr}^{-1}\left(\boldsymbol{\Omega}\right), \tag{30b}$$

$$\bar{\tilde{b}}_i \overset{N\to\infty}{\to} \text{tr}\left(\boldsymbol{R}_{1,1}\,\hat{\boldsymbol{R}}_i\right)\text{tr}^{-1}\left(\hat{\boldsymbol{R}}_i\right), \tag{30c}$$

$$\bar{\ddot{b}}_i \overset{N\to\infty}{\to} \sum_{p=2}^{L}\sum_{j=1}^{M} P_{p,j}\;\bar{\tilde{b}}_{j,p}. \tag{30d}$$

IV. Downlink Power Allocation Optimisation

A. Information-Untrusted EH

For the information-untrusted EH case, the power control aims to optimize the downlink information, energy and AN signal transmit powers at the reference cell, $\{P_{1,i}\}$, P and P_n, to maximize the worst-case ESR, $\min_i R_{S_i}$, while maintaining a minimum level of the worst-case AHE, $\bar{E}$, $\min_i E_i\left(\{P_{1,j}\},\ P,\ P_n\right) \geq \bar{E}$ and the total transmit power is within the available budget. Therefore, the corresponding optimisation problem can be formulated as[4]

$$\begin{aligned}
&\underset{\{P_{1,j}\},\ P,\ P_n}{\text{maximize}}\ \min_i R_{S_i}\\
&\text{subject to } E_i\left(\{P_{1,j}\},\ P,\ P_n\right) \geq \bar{E},\quad \forall i, &\text{(31a)}\\
&\qquad \sum_{j=1}^{M} P_{1,j} + P + P_n \leq P_t. &\text{(31b)}
\end{aligned}$$

Within the available power budget P_t, the power allocation among $\{P_{1,j}\}$, P and P_n is optimized at the reference cell, while we assume that there is no central power control among multiple cells. For simplicity we assume uniform power allocation at the interfering cells, i.e., $P_{p,i} = \frac{P_t}{M},\ \forall\ p,\ \forall\ i$.

The power control problem (31) is feasible if there exist power allocation sets $\{P_{1,i}\}$, P and P_n satisfy the constraints (31a) and (31b).

Without loss of generality, we assume that the problem in (31) is feasible and focus on solving it. It can be seen that the objective function in (31) is a complicated nonconvex function since it consists of logarithm of product of fractional functions, $\min_i \log_2[(1+\text{SINR}_{I_i})/(1+\text{SINR}_{E_i})]$, while the constraints (31a) and (31b) are convex since they are linear in terms of the optimization variables. The objective function can be convexified as follows. First, using (13), (15), (17), (19) and certain logarithmic properties, we can replace the objective function $\min_i R_{S_i}$ in (31) with the monotonically increasing expression, $\min_i R''_{S_i} = \min_i[(1+\text{SINR}_{I_i})/(1+\text{SINR}_{E_i})]$, given in (32)[5] at the bottom of this page. Second, the new objective expression $\min_i R''_{S_i}$ is still nonconvex, therefore, we use exponential variable substitution method [32], [23], [33] to convert $\min_i R''_{S_i}$ into an equivalent linear expression as follows: Let us substitute the multiplicative terms in the denominators and numerators in (32) by exponential slack variables:

$$\begin{aligned}
e^{u_i} &= P_{1,i}\left(\bar{a}_{i,i}^{(1)} + \bar{\tilde{a}}_i\right) + \sum_{j\neq i} P_{1,j}\;\bar{a}_{i,j}^{(1)}\\
&\quad + P\;\bar{a}_{1_i} + P_n\;\bar{a}_i + \bar{\hat{a}}_i + \sigma_n^2,\quad \forall\ i, &\text{(34a)}\\
e^{s_i} &= P_{1,i}\bar{\tilde{a}}_i + \sum_{j\neq i} P_{1,j}\;\bar{a}_{i,j}^{(1)} + P\;\bar{a}_{1_i} + P_n\bar{a}_i + \bar{\hat{a}}_i + \sigma_n^2,\quad \forall\ i, &\text{(34b)}\\
e^{t_i} &= P_{1,i}\;\bar{b}_{i,1} + P\;\bar{b} + P_n\bar{b}_i + \bar{\hat{b}}_i + \sigma_n^2,\quad \forall\ i, &\text{(34c)}\\
e^{v_i} &= P\;\bar{b} + P_n\bar{b}_i + \bar{\hat{b}}_i + \sigma_n^2,\quad \forall\ i. &\text{(34d)}
\end{aligned}$$

[4]Considering the worst-case scenario is relevant since the EH can attack any IU.

[5]Since the logarithmic and exponential functions are monotonically increasing in their arguments, i.e., $f(x_1) > f(x_2)$, implies that $\log_2(f(x_1)) > \log_2(f(x_2))$ and $e^{f(x_1)} > e^{f(x_2)}$. Therefore, $\arg\max_x \log_2(f(x)) = \arg\max_x f(x)$ and $\arg\max_x e^{f(x)} = \arg\max_x f(x)$.

$$\min_i R''_{S_i} = \min_i \frac{\left(P_{1,i}\left(\bar{a}_{i,i}^{(1)} + \bar{\tilde{a}}_i\right) + \sum_{j\neq i}^{M} P_{1,j}\;\bar{a}_{i,j}^{(1)} + P\;\bar{a}_{1_i} + P_n\bar{a}_i + \bar{\hat{a}}_i + \sigma_n^2\right)\left(P\;\bar{b} + P_n\bar{b}_i + \bar{\hat{b}}_i + \sigma_n^2\right)}{\left(P_{1,i}\;\bar{\tilde{a}}_i + \sum_{j\neq i}^{M} P_{1,j}\;\bar{a}_{i,j}^{(1)} + P\;\bar{a}_{1_i} + P_n\bar{a}_i + \bar{\hat{a}}_i + \sigma_n^2\right)\left(P_{1,i}\;\bar{b}_{i,1} + P\;\bar{b} + P_n\bar{b}_i + \bar{\hat{b}}_i + \sigma_n^2\right)} \tag{32}$$

$$R''_i = \prod_i (1+\text{SINR}_{I_i}) = \prod_i \frac{\left(P_{1,i}\left(\bar{a}_{i,i}^{(1)} + \bar{\tilde{a}}_i\right) + \sum_{j\neq i}^{M} P_{1,j}\;\bar{a}_{i,j}^{(1)} + P\;\bar{a}_{1_i} + P_n\;\bar{a}_i + \bar{\hat{a}}_i + \sigma_n^2\right)}{\left(P_{1,i}\;\bar{\tilde{a}}_i + \sum_{j\neq i}^{M} P_{1,j}\;\bar{a}_{i,j}^{(1)} + P\;\bar{a}_{1_i} + P_n\;\bar{a}_i + \bar{\hat{a}}_i + \sigma_n^2\right)} \tag{33}$$

Using the previous substitutions and some of the logarithmic and exponential properties, we can write the objective function as $\min_i (u_i - s_i - t_i + v_i)$. To keep the maximization of our objective bounded, we have to ensure that the slack variables u_i, s_i, t_i and v_i are within the values of their substituted expressions in (34a)–(34d), respectively. Therefore, (31) is recast as

$$\begin{aligned}
&\underset{\substack{\{P_{1,j}\},\ P,\ P_n,\\ \{u_i,s_i,t_i,v_i\}}}{\text{maximize}} \quad \min_i (u_i - s_i - t_i + v_i)\\
&\text{subject to } P_{1,i}\left(\bar{a}_{i,i}^{(1)} + \bar{\bar{a}}_i\right) + \sum_{j\neq i} P_{1,j}\ \bar{a}_{i,j}^{(1)}\\
&\qquad + P\ \bar{a}_{1_i} + P_n\ \bar{a}_i + \bar{\hat{a}}_i + \sigma_n^2\\
&\qquad \geq e^{u_i}, \quad \forall\ i, \qquad (35a)\\
&\qquad P_{1,i}\ \bar{\bar{a}}_i + \sum_{j\neq i} P_{1,j}\ \bar{a}_{i,j}^{(1)} + P\ \bar{a}_{1_i} + P_n\ \bar{a}_i + \bar{\hat{a}}_i + \sigma_n^2\\
&\qquad \leq e^{\bar{s}_i}\left(s_i - \bar{s}_i + 1\right), \quad \forall\ i, \qquad (35b)\\
&\qquad P_{1,i}\ \bar{b}_{i,1} + P\ \bar{b} + P_n\bar{b}_i + \bar{\bar{b}}_i + \sigma_n^2\\
&\qquad \leq e^{\bar{t}_i}\left(t_i - \bar{t}_i + 1\right), \quad \forall\ i \qquad (35c)\\
&\qquad P\ \bar{b} + P_n\bar{b}_i + \bar{\bar{b}}_i + \sigma_n^2 \geq e^{v_i}, \quad \forall\ i, \qquad (35d)\\
&\qquad (31a),\ (31b). \qquad (35e)
\end{aligned}$$

In constraints (35b) and (35c), e^{s_i} and e^{t_i} are linearized as $e^{s_i} = e^{\bar{s}_i}(s_i - \bar{s}_i + 1)$ and $e^{t_i} = e^{\bar{t}_i}(t_i - \bar{t}_i + 1)$ to avoid having convex downward function being bounded below, where $\bar{s}_i$ and $\bar{t}_i$ are the points around which the linearizations are made. Now, the reformulated problem (35) is convex and can be solved iteratively using any convex optimization software such as CVX [34]. After each iteration, the values of $\bar{s}_i$ and $\bar{t}_i$ (which are initialized for the first iteration) are updated by the optimized values of s_i and t_i, respectively. The iterative optimization process continues until the errors $\{|s_i - \bar{s}_i|\}$ and $\{|t_i - \bar{t}_i|\}$ fall below a certain tolerance.

B. Information-Trusted EH

For information-trusted EH, the power control aims to optimize the downlink information and energy signal transmit powers at the reference cell, $\{P_{1,i}\}$ and P, to maximize the ergodic sum-rate, $\sum_i R_i$, while maintaining the total transmit power $\leq P_t$ and a minimum level of the AHE, $\bar{E}$, $E_{\mathcal{M}}(\{P_{1,j}\},\ P,\ P_n) \geq \bar{E}$, where $E_{\mathcal{M}}$ is the AHE by the EH when attacking the IUs whose indices are specified by $\mathcal{M}$. The right-hand side expression in (21) is valid to calculate $E_{\mathcal{M}}$ ($i \sim \mathcal{M}$, i.e., attacking the $\mathcal{M}$ IUs instead of attacking $\text{IU}_{1,i}$). Therefore, the corresponding optimisation problem can be formulated as[6]

$$\begin{aligned}
&\underset{\{P_{1,j}\},\ P}{\text{maximize}} \quad \sum_i R_i\\
&\text{subject to } E_{\mathcal{M}} \geq \bar{E}, \quad \forall i, \qquad (36a)\\
&\qquad \sum_{j=1}^{M} P_{1,j} + P \leq P_t. \qquad (36b)
\end{aligned}$$

[6]Considering the ergodic sum-rate maximization problem is relevant since the EH can harvest energy from all IUs signals. In addition, AN jamming is not taken ($P_n = 0$) since the EH is information-trusted.

To convexify (36), we follow comparable steps to those used to reformulate problem (31) in the previous subsection. Using (13)–(15) and some logarithmic properties, we can replace $\sum_i R_i$ in the objective function of (36) with the monotonically increasing expression, $R_i'' = \prod_i (1 + \text{SINR}_{I_i})$, given in (33), as shown at the bottom of the previous page. Then, by applying exponential variable substitution as in the previous subsection, we can recast (36) as in (37)

$$\begin{aligned}
&\underset{\{P_{1,j}\},\ P_1,\ \{u_i,s_i\}}{\text{maximize}} \quad \sum_i (u_i - s_i)\\
&\text{subject to } P_{1,i}\left(\bar{a}_{i,i}^{(1)} + \bar{\bar{a}}_i\right) + \sum_{j\neq i} P_{1,j}\ \bar{a}_{i,j}^{(1)} + P\ \bar{a}_{1_i} + \bar{\hat{a}}_i + \sigma_n^2\\
&\qquad \geq e^{u_i}, \quad \forall i, \qquad (37a)\\
&\qquad P_{1,i}\ \bar{\bar{a}}_i + \sum_{j\neq i} P_{1,j}\ \bar{a}_{i,j}^{(1)} + P\ \bar{a}_{1_i} + \bar{\hat{a}}_i + \sigma_n^2\\
&\qquad \leq e^{\bar{s}_i}\left(s_i - \bar{s}_i + 1\right), \quad \forall\ i, \qquad (37b)\\
&\qquad (36a), (36b). \qquad (37c)
\end{aligned}$$

Problem (37) is convex and can be solved iteratively in the same fashion as the problem in problem (35). In the next section, we analyze the complexity of our proposed algorithms.

V. Complexity Analysis

The computational complexity of the downlink transmission is related to the complexities of evaluating the asymptotic values in (27)-(30) which are dominated by the $N \times N$ matrix multiplication which has an $\mathcal{O}\left(N^3\right)$ asymptotic complexity [35], and the complexity of the power allocation optimization. The complexity of problems (35) and (37) depends on the number of constraints, optimization variables and the size of the input data of the optimization problems in thier standard linear programming (LP) forms. Note that the solvers that are based on symmetric primal-dual interior-point algorithm (such as those supported by CVX software like SDPT3 and SeDuMi) do not support constraints that involve entropy family function like the exponential function e^{u_i} in (35) [34], [36], [37]. Therefore, all the exponential functions are linearized internally by the optimization software solver as $e^{u_i} = e^{\bar{u}_i}(u_i - \bar{u}_i + 1)$, $e^{v_i} = e^{\bar{v}_i}(v_i - \bar{v}_i + 1)$, $\forall i$. $\bar{u}_i$ and $\bar{v}_i$ are the points around which the linearization are made. To calculate the complexity of per-iteration problem for the formulation in (35), we need to recast (35) in a standard LP form by rewriting the min operator in the objective function $\min_i (u_i - s_i - t_i + v_i)$. This can be done by replacing the objective function with new slack variable π and introducing the constraint $(u_i - s_i - t_i + v_i) \geq \pi,\ \forall\ i$. Therefore, (35) will be

$$\begin{aligned}
(P_{\text{st}}): \quad &\underset{\substack{\{P_{1,j}\},\ P,\ P_n,\\ \{u_i,s_i,t_i,v_i\},\ \pi}}{\text{maximize}} \quad \pi \qquad (38a)\\
&\text{subject to } (u_i - s_i - t_i + v_i) \geq \pi, \quad \forall\ i, \qquad (38b)\\
&\qquad (35a) - (35e). \qquad (38c)
\end{aligned}$$

With the LP formulation in (38) (which is equivalent to (35)), we follow the procedure described in Chapter 6 in [38] to calculate the computational complexity of

finding a solution for (35) within an accuracy ϵ in terms of the following parameters: number of the real design variables, $n_v = 5M + 3$; total number of per-scalar value constraints, $n_c = 6M + 1$; the 1-norm of the input data vector, $\|\text{data}(P_{\text{st}})\|_1$, $\text{data}(P_{\text{st}}) = [n_v,\ n_c,\ [\bar{u}_1,\ \bar{s}_1,\ \bar{t}_1,\ \bar{v}_1;\ \ldots;\ \bar{u}_M, \bar{s}_M, \bar{t}_M, \bar{v}_M],\ \sigma_n^2,\ P_t,\ \bar{E}]$; and total number of input data, $\dim \text{data}(P_{\text{st}}) = 4M+5$. Having these parameters, with $\mathcal{O}(1)$ complexity per real operation, the complexity of getting a solution for P_{st} within an accuracy ϵ, is [38]

$$\begin{aligned}&\text{Comp}\,(P_{\text{st}}, \epsilon)\\ &\quad = (n_v + n_c)^{\frac{3}{2}}\, n_v^2\\ &\qquad \times \ln\left(\frac{\dim \text{Data}\,(P_{\text{sub}}) + \|\text{Data}\,(P_{\text{sub}})\|_1 + \epsilon^2}{\epsilon}\right). \quad (39)\end{aligned}$$

The result in (39) has an asymptotic complexity of $\mathcal{O}\left(M^{\frac{7}{2}}\left[\ln(M) + \ln(\frac{1}{\epsilon})\right]\right)$. The optimization complexity does not depend on the number of transmit antenna N since the optimization is per user signal power.

VI. Simulation Results and Evaluations

This section provides numerical examples to demonstrate the system asymptotic performance. In our simulations, the system parameters are selected as follows: the number of transmit antennas per cell is $N = 512$, the number of cells is $L = 3$ and the number of IUs per cell is $M = 3$. Both the IUs and the EH are assumed to have 30 dB path-loss to their local BSs which corresponds to $\gamma_1 = 10^{-3}$, and 70 dB path-loss to the neighbouring cell BSs, which corresponds to $\gamma_2 = 10^{-7}$. The variance of the thermal noise at all users and the BSs' receivers is $\sigma_n^2 = 10^{-3}$. The correlation matrices, $\mathcal{R}_I$ and $\mathcal{R}_E$, are generated using the Truncated Laplacian PAS model which is suitable for the outdoor macrocell environment [39], with a mean AoA varying randomly for different users across the interval $[-\pi,\ \pi]$. The total power budget at every BS is $P_t = 1W$. The energy harvesting efficiency is dependent on the incident power range at the receving antennas [40], accordingly, it is assumed to be equal for all EHs as $\zeta = 0.5$, and this is reasonable for the expected incident power range from -5 dBm to 5 dBm. The average training signal power per user is fixed at $P_I = P_E = 1\ W$.

To demonstrate the performance of the jointly optimized worst-case ESR, $\min_i R_{S_i}$, and worst-case AHE, $\min_i E_i$, we use the energy-secrecy (E-R$_{\text{S}}$) region plot which shows the optimal $\min_i R_{S_i}$ against the constraint on $\min_i E_i$, $\bar{E}$. For no constraint on the worst-case AHE, $\bar{E} = 0$, the BS has the freedom to optimize the information, AN and energy signal transmissions such that $\min_i R_{S_i}$ is at its maximum. Conversely, as $\bar{E}$ increases, more power is devoted to satisfy the worst-case AHE constraint, $\min_i E_i \geq \bar{E}$, until $\min_i R_{S_i} = 0$ at the end of the E-R$_{\text{S}}$ region. Therefore, the larger the area under the E-R$_{\text{S}}$ region the better the performance.

Fig. 1 shows a 3-D plot representing the E-R$_{\text{S}}$ regions obtained by solving (35) at different values of ϕ. Generally, during the intervals of low worst-case AHE constraints, the E-R$_{\text{S}}$ regions show no tradeoff between $\min_i R_{S_i}$ and $\min_i E_i$, i.e., the received information and AN signals are sufficient to provide the EH with the required worst-case AHE. As the worst-case AHE constraints increase, the BS trades some of the secrecy performance for satisfying the AHE constraints. As expected, the optimized worst-case ESR decreases as $\bar{E}$ increases.

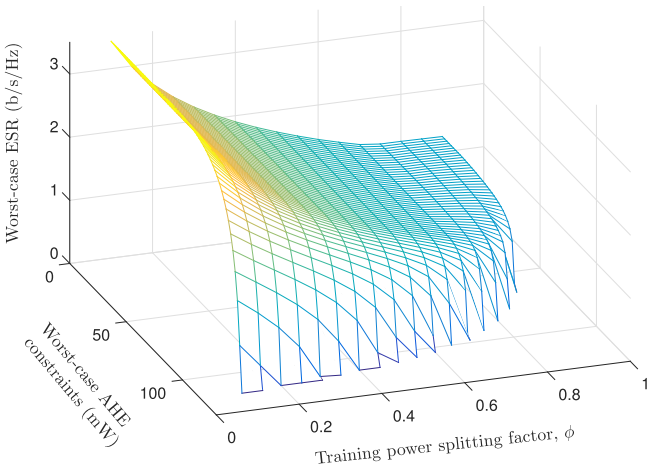

Fig. 1. E-R$_{\text{S}}$ regions versus the training power splitting factor.

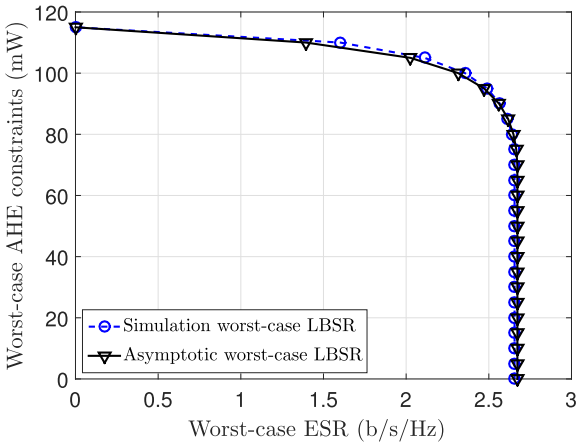

Fig. 2. E-R$_{\text{S}}$ region for the information-untrusted EH, $\phi = 0.2$.

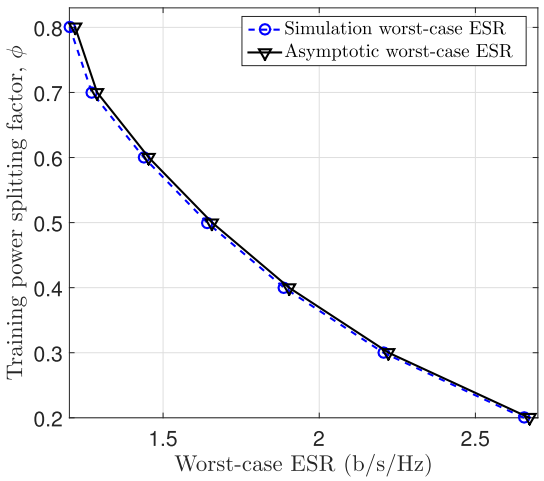

Fig. 3. Worst-case ESR versus a range of training power splitting factor, $\bar{E} = 60\ mW$.

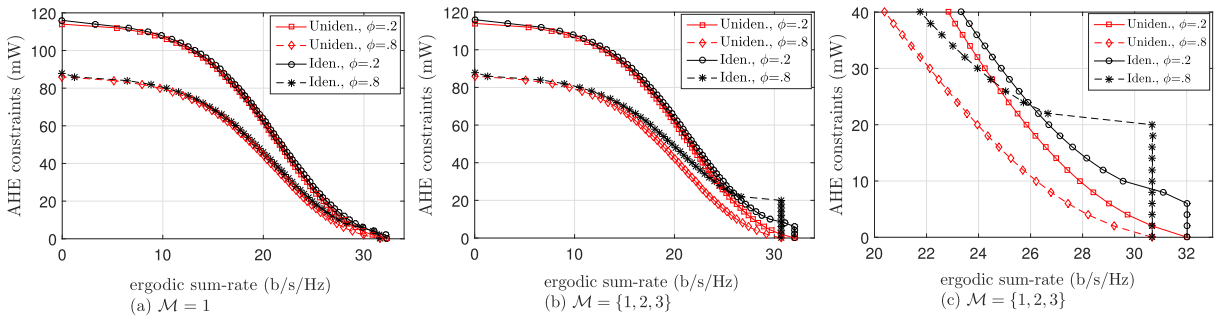

Fig. 4. E-R regions for the information-trusted EH for different values of $\mathcal{M}$.

Fig. 2 compares the asymptotic E-R$_S$ region (at $\phi = 0.2$) obtained by solving (35) using the asymptotic values of $\{\bar{a}_{i,i}^{(1)}, \bar{a}_{i,j}^{(p)}, \bar{\tilde{a}}_i, \bar{a}_{1_i}, \bar{a}_i, \bar{\hat{a}}_i\}$, $\{\bar{b}_{i,p}, \bar{b}, \bar{b}_i, \bar{\tilde{b}}_i\}$ and $\{\bar{\tilde{b}}_{j,p}, \bar{\tilde{b}}, \bar{\tilde{b}}_i, \bar{\ddot{b}}_i\}$, with the E-R$_S$ region obtained by solving (35) using the simulation average values of $\{\bar{a}_{i,i}^{(1)}, \bar{a}_{i,j}^{(p)}, \bar{\tilde{a}}_i, \bar{a}_{1_i}, \bar{a}_i, \bar{\hat{a}}_i\}$, $\{\bar{b}_{i,p}, \bar{b}, \bar{b}_i, \bar{\tilde{b}}_i\}$ and $\{\bar{\tilde{b}}_{j,p}, \bar{\tilde{b}}, \bar{\tilde{b}}_i, \bar{\ddot{b}}_i\}$. The results give an insight into the accuracy of our asymptotic analysis. Fig. 3 compares the asymptotic and the simulation performances of worst-case ESR versus training power splitting factor, ϕ. AS expected, the worst-case ESR decreases as ϕ increases.

For the information-trusted EH case, similar to the E-R$_S$ region, we use the energy-rate (E-R) region which defines the tradeoff between the AHE ($E_{\mathcal{M}}$), and the ergodic sum-rate, $\sum_i R_i$ by solving (37). We assume two scenarios of information-trusted EH case: in the first scenario, the reference BS is able to detect the active eavesdropping attack and to identify the attacker, the EH, therefore, $E_{\mathcal{M}}$ is calculated by (21); in the second scenario, the reference BS is able to detect the active eavesdropping attack, however, it can not identify the attacker, therefore, $E_{\mathcal{M}}$ is calculated as $E_{\mathcal{M}} = \zeta(\sum_j P_{1,j}\ \bar{\tilde{b}}_{j,p} + P\bar{\tilde{b}} + P_n\bar{\tilde{b}}_i + \bar{\ddot{b}}_i)$, where $i \sim \mathcal{M}$. Fig. 4 demonstrates the E-R regions for both scenarios, the identified and the unidentified attacker, for the following parameters: two sets of attacked IUs, $\mathcal{M} = 1$ and $\mathcal{M} = \{1,\ 2,\ 3\}$; and $\phi = 0.2,\ 0.8$. In the first sub-plot, (a), the EH attacks one IUs, IU$_{1,1}$. The tradeoff between the ergodic sum-rate and the AHE is clear as expected, where the ergodic sum-rate decreases as the AHE constraint increases. However, the performance gap between the identified and unidentified attacker scenarios is small. In the second sub-plot, (b), in which the EH attacks multiple IUs, $\mathcal{M} = \{1,\ 2,\ 3\}$, it can be noticed that identifying the attacker by the BS can help in improving the worst-case ergodic sum-rate, particularly at low AHE constraints region. The third sub-plot, (c), emphasizes the performance gap between the identified and unidentified attacker scenarios. For example, at $\phi = 0.8$, identifying the attacker will gain 5 $b/s/Hz$ in the ergodic sum-rate performance for a AHE of 20 mW.

In Fig. 5, we demonstrate the energy harvesting performance of the EH. The figure focuses on the effect of balancing the limited training power between the legitimate energy harvesting, $(1-\phi)P_E$, and harvesting energy through eavesdropping, ϕP_E, on the total AHE by the EH. At small power splitting factors (as $\phi = 0.1$), most of the training

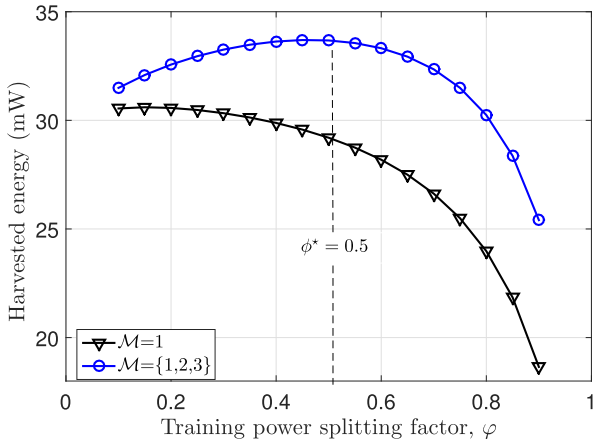

Fig. 5. Harvested energy versus ϕ.

power is invested in the legitimate channel estimation and therefore most of the harvested energy is via the signal aligned to the legitimate channel $\boldsymbol{g}_1$. Increasing the eavesdropping training power (by increasing ϕ) results in an increase in the AHE dominated by the average harvested energy from the legitimate signal $\zeta(\sum_j P_{1,j}\ \bar{\tilde{b}}_{j,p} + P\bar{\tilde{b}} + P_n\bar{\tilde{b}}_i + \bar{\ddot{b}}_i)$ and the average harvested energy from the eavesdropped signal $\zeta(\sum_j P_{1,j}\ \bar{b}_{j,p} + P\bar{b} + P_n\bar{b}_i + \bar{\hat{b}}_i)$ until a point $\phi^\star$—the point corresponding to the maximum harvested energy—beyond which the harvested energy decreases with increasing ϕ. $\phi^\star$ gives the optimal balance between the legitimate and the eavesdropping training power for maximizing the AHE.

Fig. 6 shows the achievable worst-case ESR versus the number of transmit antennas which varies over the range $N = [5,\ 20,\ 50,\ 100,\ 300, \ldots,\ 1700]$. As expected, as the number of transmit antennas increases, the worst-case ESR increases.

Fig. 7 shows the convergence speed of the power allocation iterative LP problem in (37). Since the iterative process is based on updating the initial values of Taylor first order approximations $\{\bar{s}_i\}$ in (37b), therefore, the convergence speed is affected by the choice of the initial values $\{\bar{s}_i\}$. Intuitively, the initial values can be calculated with the following formula

$$\bar{s}_i = \log\left[\frac{P_t - P_n}{M+1}\left(\bar{\tilde{a}}_i + \sum_{\substack{j=1\\ j\neq i}}^{M} \bar{a}_{i,j}^{(1)}\right) + P\,\bar{a}_{1_i} + \bar{\hat{a}}_i + \sigma_n^2\right], \quad \forall i. \tag{40}$$

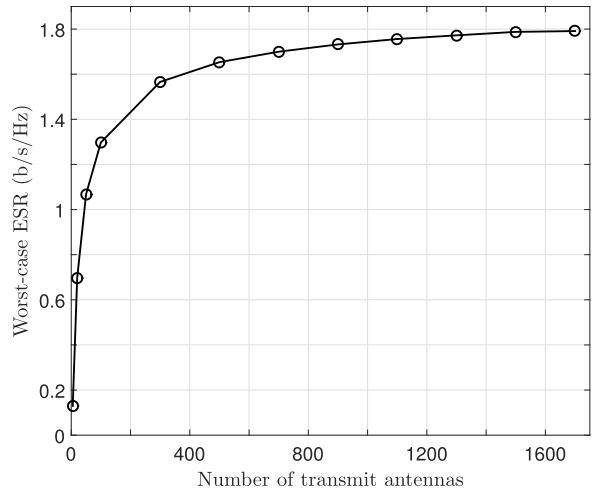

Fig. 6. The worst-case ESR versus the number of transmit antennas, $\phi = 0.5$, $\bar{E} = 0$.

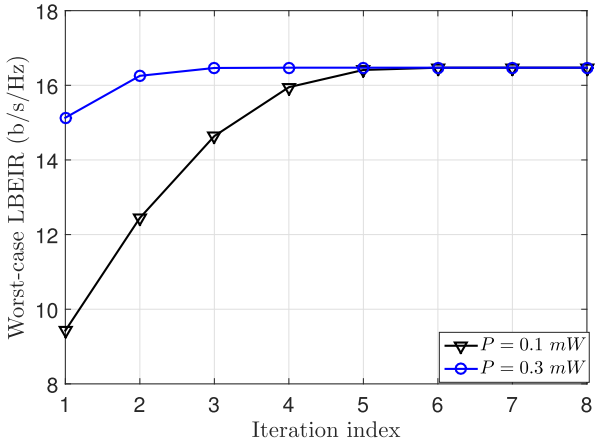

Fig. 7. Convergence speed of the iterative power allocation optimization.

In (40), we assume uniform power allocation among the information and energy signals. Good initial value approximations can be found via one-dimensional search across $0 \leq P \leq P_t$. Fig. 7 shows the convergence of the ergodic sum-rate per iteration with the initial values generated by (39) with $P = 0.1$, $0.3\ W$, $\mathcal{M} = 1$ and at a point within the tradeoff region corresponding to $\bar{E} = 80\ mW$. The results in the figure show different convergence speeds for different initializations. For the initialization with $P = 0.1\ W$, the iterative algorithm converges to its final optimal objective after 5 iterations, while via the initialization with $P = 0.3\ W$, the iterative algorithm reaches its final optimal objective after 3 iterations.

VII. Conclusions

We optimized the downlink transmission for SWIPT to maximize the worst-case ESR of the IUs under a constraint on worst-case AHE by the active two antennas EH in multi-cell massive MIMO systems. The EH has the potential to harvest energy via one antenna and to eavesdrop an information signal via the other antenna. The considered problems were: 1) The maximisation of the worst-case ESR under a constraint on the worst-case AHE by the EH for the case of information-untrusted EH; 2) The maximisation of the ergodic sum-rate of the IUs under a constraint on the worst-case AHE by the EH for the case of information-untrusted EH. Asymptotic expressions for ergodic sum-rate, ESR and AHE were derived in a large system limit. Then, we used these results to optimize power allocation for downlink SWIPT transmissions which include: information signals, AN and energy signal towards the IUs, legitimate and illegitimate antennas of the EH, respectively. Our results demonstrate the performances of SWIPT over the E-Rs and E-R tradeoff regions. Also, the impact of the combined legitimate/illegitimate operation of the EH on the SWIPT performance has been investigated. Considering the same problem for multi-antenna users and cell-free scenario is left as a further work.

Appendix A

A. Proof of Lemma 1

Given that $\{\rho(\boldsymbol{R}_{i,l,1}),\ \rho(\boldsymbol{R}_{1,1})\} \leq c \leq \infty$ and by using Corollary 1, we have

$$\tilde{\boldsymbol{h}}_{i,l,1}^H \boldsymbol{R}_{i,l,1}^{\frac{1}{2}} \boldsymbol{R}_{i,p,1}^{\frac{1}{2}} \tilde{\boldsymbol{h}}_{i,p,1} \overset{N\to\infty}{\to} \begin{cases} \mathrm{tr}\left(\boldsymbol{R}_{i,p,1}\right), & \text{for } l = p \\ 0, & \text{for } l \neq p. \end{cases} \tag{41}$$

Therefore, by expanding the product $\boldsymbol{y}_{1,i}^H \boldsymbol{y}_{1,i}^H$ using (4) followed by applying Corollary 1, we get

$$\left[\boldsymbol{y}_{1,i}^H \boldsymbol{y}_{1,i}\right] \overset{N\to\infty}{\to} \begin{cases} \tau^2 P_I \sum_{l=1}^{L} \mathrm{tr}\left(\boldsymbol{R}_{i,l,1}\right) + \tau^2 P_E \mathrm{tr}\left(\boldsymbol{R}_{1,1}\right) & \\ +N\tau\sigma_n^2, & i \in \mathcal{M} \\ \tau^2 P_I \sum_{l=1}^{L} \mathrm{tr}\left(\boldsymbol{R}_{i,l,1}\right) + N\tau\sigma_n^2, & i \notin \mathcal{M}, \end{cases} \tag{42}$$

and

$$\frac{\boldsymbol{y}_{1,i}^H \boldsymbol{y}_{1,i} - \tau^2 P_I \sum_t \mathrm{tr}\left(\boldsymbol{R}_{i,t,1}\right) + N\tau\sigma_n^2}{\tau^2 \mathrm{tr}\left(\boldsymbol{R}_{1,1}\right)} \overset{N\to\infty}{\to} \begin{cases} \phi_1 P_E, & i \notin \mathcal{M} \\ 0, & i \notin \mathcal{M}. \end{cases} \tag{43}$$

This concludes the proof.

B. Proof of Lemma 2

The correlation matrix $\boldsymbol{R}_{1,p}$ belongs to the family of Hermitian Toeplitz matrices and is defined as $\boldsymbol{R}_{1,p} = \boldsymbol{R}_N\left(r_{m,n}\right) = [r_{m,n} = r_{m-n};\ m,n = 0,1,\ldots,N-1]$,

$$\boldsymbol{R}_N = \begin{bmatrix} r_{1-1} & r_{1-2} & \cdots & r_{1-N} \\ r_{2-1} & r_{2-2} & \cdots & \\ \vdots & & \ddots & \vdots \\ r_{N-1} & & \cdots & r_{N-N} \end{bmatrix}, \tag{44}$$

where the correlation coefficients $r_{m,n}$ are generated using the truncated Laplacian model[7] [39]

$$r_{m,n}\left(d,\phi_0\right) = \int_{-\pi}^{\pi} \gamma_t\, e^{\frac{j2\pi(m-n)d\ \ sin(\phi-\phi_0)}{\lambda}}\, \bar{P}\left(\phi-\phi_0\right) d\phi, \tag{45}$$

d is the spacing between successive antennas, $j = \sqrt{-1}$ (for this equation only), λ is the signal wavelength, ϕ is the angle of

[7]We assume a uniformly linear antenna array with a truncated range of AoA $[-\pi,\ \pi]$.

arrival (AoA) of the signal path, ϕ_0 is the mean AoA over all signal paths and it varies from one user to another, $\bar{P}(\phi-\phi_0)$ is the power angular spectrum which follows a truncated Laplacian distribution. By making use of Lemma 4.1 in [41], the spectral radius of the Hermitian Toeplitz matrix $\boldsymbol{R}_N(r_{m,n})$ is upper bounded by the supremum of the generating function

$$\rho\left(\boldsymbol{R}_N\left(r_{m,n}\right)\right) \leq \sup r_{m,n}\left(d,\phi_0\right). \tag{46}$$

Knowing that for truncated Laplacian distribution $\int_{-\pi}^{\pi}\bar{P}(\phi-\phi_0)d\phi = 1$, $\sup r_{m,n}(d,\phi_0)$ is found by the extreme case of signal autocorrelation at one antenna, i.e., at $n=m$. Therefore, $\sup r_{m,n}(d,\phi_0) = r_{m,n=m}(d,\phi_0) = \gamma_1$ and then

$$\rho\left(\boldsymbol{R}_N\left(r_{m,n}\right)\right) \leq \gamma_1. \tag{47}$$

The spectral boundedness of $\boldsymbol{R}_{i,l,p}$ can be proved by following the same steps. This concludes the proof.

C. Proof of Lemma 3

Let us put $\boldsymbol{C}_{p,i}$ as $\sqrt{P_I}\boldsymbol{R}_{i,p,p}(\boldsymbol{B}_i+\sigma_n^2\boldsymbol{I}_N)^{-1}$. By making use of the eigenvalue decomposition definition, it is easy to verify that $\rho(\boldsymbol{B}_i+\sigma_n^2\boldsymbol{I}_N)\geq\sigma_n^2$, and therefore, the matrix inverse imposes that $\rho(\boldsymbol{B}_i+\sigma_n^2\boldsymbol{I}_N)^{-1}\leq\frac{1}{\sigma_n^2}$. Since $\rho(\boldsymbol{R}_{i,p,p})\leq c\leq\infty$, where c is a positive real constant, then, by applying Lemma 4 we have

$$\rho\left(\boldsymbol{C}_{p,i}\right)\leq c\leq\infty. \tag{48}$$

The proof of $\rho\left(\boldsymbol{C}_i\right)\leq c\leq\infty$ can be done in a comparable way. This concludes the proof.

D. Proof of Lemma 4

By making use of Corollary 11 in [42] (which relates the spectral radius of product of matrices to their individual spectral radii), we have

$$\rho\left(\prod_m A_m\right)\leq\prod_m\rho\left(A_m\right). \tag{49}$$

Since $\{A_m\}$ is of a finite length and $\rho(A_m)<\infty$, $\forall\ m$, then $\rho(\prod_m A_m)\leq\prod_m\rho(A_m)<\infty$. This concludes the proof.

E. Proof of Lemma 5

Defining $\mathbb{I}=\{i\}\times\{j\}$, we have

$$\begin{aligned}
&E\left[\left|\boldsymbol{x}^H\boldsymbol{A}\boldsymbol{y}\right|^2\right]\\
&=E\left[\left|\sum_{\mathbb{I}}\boldsymbol{x}_i^H\boldsymbol{\Theta}_i^H\boldsymbol{A}\bar{\boldsymbol{\Theta}}_j\boldsymbol{y}_j\right|^2\right]\\
&=\sum_{\mathbb{I}}E\left[\left|\boldsymbol{x}_i^H\boldsymbol{\Theta}_i^H\boldsymbol{A}\bar{\boldsymbol{\Theta}}_j\boldsymbol{y}_j\right|^2\right]\\
&\quad+\sum_{\substack{\mathbb{I}\times\mathbb{I}\\ \{i,j\}\neq\{m,n\}}}E\left[\left\langle\boldsymbol{x}_i^H\boldsymbol{\Theta}_i^H\boldsymbol{A}\bar{\boldsymbol{\Theta}}_j\boldsymbol{y}_j,\ \boldsymbol{x}_m^H\boldsymbol{\Theta}_m^H\boldsymbol{A}\bar{\boldsymbol{\Theta}}_n\boldsymbol{y}_n\right\rangle\right],
\end{aligned} \tag{50}$$

$$\begin{aligned}
&E\left[\left|\boldsymbol{x}_i^H\boldsymbol{\Theta}_i^H\boldsymbol{A}\bar{\boldsymbol{\Theta}}_j\boldsymbol{y}_j\right|^2\right]\\
&=\boldsymbol{x}_i^H\boldsymbol{\Theta}_i^H\boldsymbol{A}\bar{\boldsymbol{\Theta}}_jE\left[\boldsymbol{y}_j\boldsymbol{y}_j^H\right]\bar{\boldsymbol{\Theta}}_j^H\boldsymbol{A}^H\boldsymbol{\Theta}_i\boldsymbol{x}_i\\
&=\boldsymbol{x}_i^H\boldsymbol{\Theta}_i^H\boldsymbol{A}\bar{\boldsymbol{\Theta}}_j\bar{\boldsymbol{\Theta}}_j^H\boldsymbol{A}^H\boldsymbol{\Theta}_i\boldsymbol{x}_i\\
&\quad\overset{N\to\infty}{\to}\text{tr}\left(\boldsymbol{\Theta}_i^H\boldsymbol{A}\bar{\boldsymbol{\Theta}}_j\bar{\boldsymbol{\Theta}}_j^H\boldsymbol{A}^H\boldsymbol{\Theta}_i\right),
\end{aligned} \tag{51}$$

$$\begin{aligned}
&E\left[\left\langle\boldsymbol{x}_i^H\boldsymbol{\Theta}_i^H\boldsymbol{A}\bar{\boldsymbol{\Theta}}_j\boldsymbol{y}_j\ ,\ \boldsymbol{x}_m^H\boldsymbol{\Theta}_m^H\boldsymbol{A}\bar{\boldsymbol{\Theta}}_n\boldsymbol{y}_n\right\rangle\right]\\
&=\boldsymbol{x}_i^H\boldsymbol{\Theta}_i^H\boldsymbol{A}\bar{\boldsymbol{\Theta}}_jE\left[\boldsymbol{y}_j\boldsymbol{y}_n^H\right]\bar{\boldsymbol{\Theta}}_n^H\boldsymbol{A}^H\boldsymbol{\Theta}_m\boldsymbol{x}_m\ \overset{N\to\infty}{\to}0.
\end{aligned} \tag{52}$$

The expectations are moved to $\boldsymbol{y}_j\boldsymbol{y}_j^H$ and $\boldsymbol{y}_j\boldsymbol{y}_n^H$ in (51) and (52) based on the statistical independence between $\boldsymbol{y}_j$ and $\boldsymbol{x}_i$; and between $\boldsymbol{y}_j\boldsymbol{y}_n^H$ and $\{\boldsymbol{x}_i,\ \boldsymbol{x}_m\}$, respectively. The asymptotic convergences in (51) and (52) follow by applying Corollary 1. Base on (50)–(52) and some trace and Cartesian product properties, we have

$$\begin{aligned}
E\left[\left|\boldsymbol{x}^H\boldsymbol{A}\boldsymbol{y}\right|^2\right]&\overset{N\to\infty}{\to}\text{tr}\left(\boldsymbol{\Theta}_i^H\boldsymbol{A}\bar{\boldsymbol{\Theta}}_j\bar{\boldsymbol{\Theta}}_j^H\boldsymbol{A}^H\boldsymbol{\Theta}_i\right)\\
&=\text{tr}\left[\boldsymbol{A}\left(\sum_{\mathbb{I}}\bar{\boldsymbol{\Theta}}_j\bar{\boldsymbol{\Theta}}_j^H\boldsymbol{\Theta}_i\boldsymbol{\Theta}_i^H\right)\boldsymbol{A}^H\right]\\
&=\text{tr}\left(\boldsymbol{A}\left(\sum_j\bar{\boldsymbol{\Theta}}_j\bar{\boldsymbol{\Theta}}_j^H\right)\left(\sum_i\boldsymbol{\Theta}_i\boldsymbol{\Theta}_i^H\right)\boldsymbol{A}^H\right)\\
&=\text{tr}\left(\boldsymbol{A}\ E\left[\boldsymbol{y}\boldsymbol{y}^H\right]E\left[\boldsymbol{x}\boldsymbol{x}^H\right]\boldsymbol{A}^H\right).
\end{aligned} \tag{53}$$

This concludes the proof.

Appendix B
Proof of Theorem 1

We assume that the EH has full knowledge of the IUs' beamforming vectors $\{\boldsymbol{w}_{j,1}\}$ and its own channels $\{\boldsymbol{g}_{E_1},\ \boldsymbol{g}_1\}$; and is able to cancel the intra-cell interference. This results in an upper bound on the EH ergodic rate. Moreover, the IUs' signals $\{x_{j,p}\}$, the AN signal z, the energy signal $\boldsymbol{w}$, and the noise at the eavesdropping antenna of the EH are independent. As a result, given (16), we have following upper bound on the ergodic rate of the EH

$$\bar{R}_{E_i}=E\left[\log_2\left(1+\overline{\text{SINR}}_{E_i}\right)\right], \tag{54}$$

where

$$\overline{\text{SINR}}_{E_i}=\frac{P_{1,i}\left|b_{i,1}\right|^2}{P|b|^2+P_n|b_i|^2+E\left[\left|\hat{b}_i\right|^2\right]+\sigma_n^2}. \tag{55}$$

By concavity of $\log(1+x)$ and using Jensen's inequality, we obtain

$$\bar{R}_{E_i}\leq R_{E_i}=\log_2\left(1+E[\overline{\text{SINR}}_{E_i}]\right). \tag{56}$$

Using the multivariate Taylor expansion, $E[\overline{\text{SINR}}_{E_i}]=E[X_i/Y_i]$, where $X_i=P_{1,i}|b_{i,1}|^2$ and $Y_i=P|b|^2+P_n|b_i|^2+E[|\hat{b}_i|^2]+\sigma_n^2$, can be expanded as [43]

$$\begin{aligned}
&E[\overline{\text{SINR}}_{E_i}]\\
&=E\left[\frac{X_i}{Y_i}\right]=\frac{E[X_i]}{E[Y_i]}-\frac{\text{cov}(X_i,Y_i)}{(E[Y_i])^2}+\frac{\text{var}(Y_i)E[X_i]}{(E[Y_i])^3}+R.
\end{aligned} \tag{57}$$

where $R = f(\text{var}(Y_i), \text{cov}(X_i, Y_i))$ is the reminder of series expansion and is very small. Since $b_{i,1}$, b and b_i are statistically independent, then, $\text{cov}(X_i, Yi) = 0$. Moreover, according to Lemma 5 (see (50) and (52) in the proof of Lemma 5), $\text{var}(\{|b|^2, |b_i|^2\}) \overset{N\to\infty}{\to} 0$, which implies that $\text{var}(Y_i), \text{var}(R) \overset{N\to\infty}{\to} 0$. Therefore, $E[\overline{\text{SINR}}_{E_i}]$ asymptotically converges as

$$\begin{aligned} E[\overline{\text{SINR}}_{E_i}] &\overset{N\to\infty}{\to} \frac{E[X_i]}{E[Y_i]} \\ &= \frac{P_{1,i} E\left[|b_{i,1}|^2\right]}{PE\left[|b|^2\right] + P_n E\left[|b_i|^2\right] + E\left[\left|\hat{b}_i\right|^2\right] + \sigma_n^2} \\ &\triangleq \text{SINR}_{E_i}. \end{aligned} \tag{58}$$

Finally, by replacing $E[\overline{\text{SINR}}_{E_i}]$ by SINR_{E_i} in (56) above, we obtain the upper bound on the EH ergodic rate in (18). This concludes the proof.

Appendix C
Derivation of the Asymptotic Received Signal Powers

We have

$$\begin{aligned} \left\|\hat{\boldsymbol{h}}_{j,p,p}\right\| &= \left(\hat{\boldsymbol{h}}_{j,p,p}^H \hat{\boldsymbol{h}}_{j,p,p}\right)^{\frac{1}{2}} = \left(\boldsymbol{y}_{p,j}^H \boldsymbol{C}_{p,j}^H \boldsymbol{C}_{p,j} \boldsymbol{y}_{p,j}\right)^{\frac{1}{2}} \\ &\overset{N\to\infty}{\to} \text{tr}^{\frac{1}{2}}\left(\hat{\boldsymbol{R}}_{j,p,p}\right). \end{aligned} \tag{59}$$

The second equality in (59) follows from substituting $\hat{\boldsymbol{h}}_{j,p,p}$ by its value in (3), while the last asymptotic convergence is determined by expanding the product $\boldsymbol{y}_{p,j}^H \boldsymbol{C}_{p,j}^H \boldsymbol{C}_{p,j} \boldsymbol{y}_{p,j}$ followed by applying Lemmas 2-4 and Corollary 1. Given that $\text{IU}_{1,i}$ is the attacked IU, using (3), (6) and (13), $a_{i,i}^{(p)}$ can be expanded as

$$\begin{aligned} a_{i,i}^{(p)} &= \boldsymbol{h}_{i,1,p}^T \boldsymbol{w}_{i,p} \\ &= \boldsymbol{h}_{i,1,p}^T \left(\tau\sqrt{P_I}\boldsymbol{C}_{p,i}^* \boldsymbol{h}_{i,1,p}^* + \tilde{\boldsymbol{h}}_{i,p,p}^{(1)}\right) \left\|\hat{\boldsymbol{h}}_{i,p,p}\right\|^{-1} \\ &\overset{N\to\infty}{\to} \tau\sqrt{P_I} \frac{\text{tr}\left(\boldsymbol{C}_{p,i}\boldsymbol{R}_{i,1,p}\right)}{\text{tr}^{\frac{1}{2}}\left(\hat{\boldsymbol{R}}_{i,p,p}\right)} + \frac{\boldsymbol{h}_{i,1,p}^T \tilde{\boldsymbol{h}}_{i,p,p}^{(1)}}{\text{tr}^{\frac{1}{2}}\left(\hat{\boldsymbol{R}}_{i,p,p}\right)}, \end{aligned} \tag{60}$$

where

$$\tilde{\boldsymbol{h}}_{i,p,p}^{(1)} = \hat{\boldsymbol{h}}_{i,p,p}^* - \tau\sqrt{P_I}\boldsymbol{C}_{p,i}^* \boldsymbol{h}_{i,1,p}^*, \tag{61}$$

provided that the matrix $\boldsymbol{C}_{p,i}\boldsymbol{R}_{i,1,p}$ has bounded spectral radius according to Lemmas 2–4. The asymptotic convergence in (60) follows from applying Corollary 1 which implies that $\boldsymbol{h}_{i,1,p}^T \boldsymbol{C}_{p,i}^* \boldsymbol{h}_{i,1,p}^*$ is independent from the small fading randomness of $\boldsymbol{h}_{i,1,p}$ and converges to the definite value $\text{tr}(\boldsymbol{C}_{p,i}\boldsymbol{R}_{i,1,p})$. Therefore,

$$\begin{aligned} E\left[a_{i,i}^{(p)}\right] &\overset{N\to\infty}{\to} \tau\sqrt{P_I} \frac{\text{tr}\left(\boldsymbol{C}_{p,i}\boldsymbol{R}_{i,1,p}\right)}{\text{tr}^{\frac{1}{2}}\left(\hat{\boldsymbol{R}}_{i,p,p}\right)} + \frac{E\left[\boldsymbol{h}_{i,1,p}^T \tilde{\boldsymbol{h}}_{i,p,p}^{(1)}\right]}{\text{tr}^{\frac{1}{2}}\left(\hat{\boldsymbol{R}}_{i,p,p}\right)} \\ &\overset{N\to\infty}{\to} \tau\sqrt{P_I}\text{tr}\left(\boldsymbol{C}_{p,i}\boldsymbol{R}_{i,1,p}\right) \text{tr}^{-\frac{1}{2}}\left(\hat{\boldsymbol{R}}_{i,p,p}\right). \end{aligned} \tag{62}$$

The second asymptotic convergence in (62) follows from (59) and the fact that $\boldsymbol{h}_{i,1,p}^T \tilde{\boldsymbol{h}}_{i,p,p}^{(1)}$ is a zero mean random variable (this is because the vectors $\{\tilde{\boldsymbol{h}}_{i,l,p}\}$, $\boldsymbol{g}_{E_p}$ and $\boldsymbol{N}_p\boldsymbol{\psi}_i^*$ are of zero mean).

$$\begin{aligned} E\left[|\tilde{a}_i|^2\right] &= \text{var}\left(a_{i,i}^{(1)}\right) = E\left[\left|a_{i,i}^{(1)} - E\left[a_{i,i}^{(1)}\right]\right|^2\right] \\ &\overset{N\to\infty}{\to} E\left[\left|\boldsymbol{h}_{i,1,1}^T \tilde{\boldsymbol{h}}_{i,1,1}^{(1)}\right|^2\right] \text{tr}^{-1}\left(\hat{\boldsymbol{R}}_{i,1,1}\right) \\ &\overset{N\to\infty}{\to} \text{tr}\left(\boldsymbol{R}_{i,1,1}\tilde{\boldsymbol{R}}_{i,1,1}^{(1)}\right) \text{tr}^{-1}\left(\hat{\boldsymbol{R}}_{i,1,1}\right). \end{aligned} \tag{63}$$

The first asymptotic convergence in (63) results from substituting the values of $a_{i,i}^{(1)}$ and $E[a_{i,i}^{(1)}]$ provided in (60) and (62). The second asymptotic convergence follows from applying Lemma 5.

For $j \neq i$, vector $\boldsymbol{w}_{j,p}$ is a summation of $L+2$ linearly transformed statistically independent vectors which are independent of $\boldsymbol{h}_{i,1,p}$. In addition, according to Lemmas 2–4, matrices $E[\boldsymbol{w}_{j,p}\boldsymbol{w}_{j,p}^H] = \hat{\boldsymbol{R}}_{j,p,p}|\hat{\boldsymbol{h}}_{j,p,p}|^{-2}$ and $\boldsymbol{R}_{i,1,p}$ and their product are of bounded spectral radii. Therefore, Lemma 5 can be applied to calculate $E[|a_{i,j\neq i}^{(p)}|^2]$ as follows

$$\begin{aligned} E\left[\left|a_{i,j\neq i}^{(p)}\right|^2\right]_{N\to\infty} &= \left[\left|\boldsymbol{h}_{i,1,p}^H\, \boldsymbol{w}_{j,p}\right|^2\right]_{N\to\infty} \\ &\overset{N\to\infty}{\to} \text{tr}\left(\boldsymbol{R}_{i,1,p}\, \hat{\boldsymbol{R}}_{j,p,p}\right) \text{tr}^{-1}\left(\hat{\boldsymbol{R}}_{j,p,p}\right). \end{aligned} \tag{64}$$

The details of achieving the asymptotically converged values $\{\bar{a}_{1_i}, \bar{a}_i, \bar{\bar{a}}_i\}$, $\{\bar{b}_{i,p}, \bar{b}_{j\neq i,p}, \bar{b}, \bar{b}_i, \bar{\hat{b}}_i\}$ and $\{\bar{\tilde{b}}_{j,p}, \bar{\tilde{b}}, \bar{\tilde{b}}_i, \ddot{b}_i\}$ in (27e)–(27g), (28a)–(28e) and (30a)–(30d), respectively, are similar to the analysis of obtaining $\{E[a_{i,i}^{(p)}], E[|\tilde{a}_i|]^2, E[|a_{i,j\neq i}^{(p)}|^2]\}$ previously described. Therefore, due to space limitation, their detailed derivations are omitted.

References

[1] X. Zhou, B. Maham, and A. Hjorungnes, "Pilot contamination for active eavesdropping," *IEEE Trans. Wireless Commun.*, vol. 11, no. 3, pp. 903–907, Mar. 2012.

[2] J. Jose, A. Ashikhmin, T. L. Marzetta, and S. Vishwanath, "Pilot contamination and precoding in multi-cell TDD systems," *IEEE Trans. Wireless Commun.*, vol. 10, no. 8, pp. 2640–2651, Aug. 2011.

[3] L. Li, A. P. Petropulu, and Z. Chen, "MIMO secret communications against an active eavesdropper," *IEEE Trans. Inf. Forensics Security*, vol. 12, no. 10, pp. 2387–2401, Oct. 2017.

[4] Y. Wu, R. Schober, D. W. K. Ng, C. Xiao, and G. Caire, "Secure massive MIMO transmission with an active eavesdropper," *IEEE Trans. Inf. Theory*, vol. 62, no. 7, pp. 3880–3900, Jul. 2016.

[5] D. Kapetanovic, G. Zheng, and F. Rusek, "Physical layer security for massive MIMO: An overview on passive eavesdropping and active attacks," *IEEE Commun. Mag.*, vol. 53, no. 6, pp. 21–27, Jun. 2015.

[6] A. Garnaev, M. Baykal-Gursoy, and H. V. Poor, "A game theoretic analysis of secret and reliable communication with active and passive adversarial modes," *IEEE Trans. Wireless Commun.*, vol. 15, no. 3, pp. 2155–2163, Mar. 2016.

[7] A. Mukherjee and A. L. Swindlehurst, "Jamming games in the MIMO wiretap channel with an active eavesdropper," *IEEE Trans. Signal Process.*, vol. 61, no. 1, pp. 82–91, Jan. 2013.

[8] Q. Xiong, Y.-C. Liang, K. H. Li, Y. Gong, and S. Han, "Secure transmission against pilot spoofing attack: A two-way training-based scheme," *IEEE Trans. Inf. Forensics Security*, vol. 11, no. 5, pp. 1017–1026, May 2016.

[9] S. Im, J. Choi, and J. Ha, "Secret key agreement for massive MIMO systems with two-way training under pilot contamination attack," in *Proc. IEEE Globecom Workshops (GC Wkshps)*, Dec. 2015, pp. 1–6.

[10] G. Yang, C. K. Ho, R. Zhang, and Y. L. Guan, "Throughput optimization for massive MIMO systems powered by wireless energy transfer," *IEEE J. Sel. Areas Commun.*, vol. 33, no. 8, pp. 1640–1650, Aug. 2015.

[11] L. Zhao, X. Wang, and K. Zheng, "Downlink hybrid information and energy transfer with massive MIMO," *IEEE Trans. Wireless Commun.*, vol. 15, no. 2, pp. 1309–1322, Feb. 2016.
[12] X. Wang and C. Zhai, "Simultaneous wireless information and power transfer for downlink multi-user massive antenna-array systems," *IEEE Trans. Commun.*, vol. 65, no. 9, pp. 4039–4048, Sep. 2017.
[13] L. Wang, K.-K. Wong, M. Elkashlan, A. Nallanathan, and S. Lambotharan, "Secrecy and energy efficiency in massive MIMO aided heterogeneous C-RAN: A new look at interference," *IEEE J. Sel. Topics Signal Process.*, vol. 10, no. 8, pp. 1375–1389, Dec. 2016.
[14] J. Zhang, C. Yuen, C.-K. Wen, S. Jin, K.-K. Wong, and H. Zhu, "Large system secrecy rate analysis for SWIPT MIMO wiretap channels," *IEEE Trans. Inf. Forensics Security*, vol. 11, no. 1, pp. 74–85, Jan. 2016.
[15] J. Zhu, Y. Li, N. Wang, and W. Xu, "Wireless information and power transfer in secure massive MIMO downlink with phase noise," *IEEE Wireless Commun. Lett.*, vol. 6, no. 3, pp. 298–301, Jun. 2017.
[16] Y. Zhu, L. Wang, K.-K. Wong, S. Jin, and Z. Zheng, "Wireless power transfer in massive MIMO-aided HetNets with user association," *IEEE Trans. Commun.*, vol. 64, no. 10, pp. 4181–4195, Oct. 2016.
[17] S. Lee, Y. Zeng, and R. Zhang, "Retrodirective multi-user wireless power transfer with massive MIMO," *IEEE Wireless Commun. Lett.*, vol. 7, no. 1, pp. 54–57, Feb. 2018.
[18] S. Kashyap, E. Björnson, and E. G. Larsson, "On the feasibility of wireless energy transfer using massive antenna arrays," *IEEE Trans. Wireless Commun.*, vol. 15, no. 5, pp. 3466–3480, May 2016.
[19] J. Zhu, R. Schober, and V. K. Bhargava, "Linear precoding of data and artificial noise in secure massive MIMO systems," *IEEE Trans. Wireless Commun.*, vol. 15, no. 3, pp. 2245–2261, Mar. 2016.
[20] M. R. A. Khandaker and K.-K. Wong, "Masked beamforming in the presence of energy-harvesting eavesdroppers," *IEEE Trans. Inf. Forensics Security*, vol. 10, no. 1, pp. 40–54, Jan. 2015.
[21] D. W. K. Ng, E. S. Lo, and R. Schober, "Robust beamforming for secure communication in systems with wireless information and power transfer," *IEEE Trans. Wireless Commun.*, vol. 13, no. 8, pp. 4599–4615, Aug. 2014.
[22] L. Liu, R. Zhang, and K.-C. Chua, "Secrecy wireless information and power transfer with MISO beamforming," *IEEE Trans. Signal Process.*, vol. 62, no. 7, pp. 1850–1863, Apr. 2014.
[23] M. Alageli, A. Ikhlef, and J. Chambers, "Optimization for maximizing sum secrecy rate in MU-MISO SWIPT systems," *IEEE Trans. Veh. Technol.*, vol. 67, no. 99, pp. 537–553, Jan. 2017.
[24] H. Q. Ngo, E. G. Larsson, and T. L. Marzetta, "Energy and spectral efficiency of very large multiuser MIMO systems," *IEEE Trans. Commun.*, vol. 61, no. 4, pp. 1436–1449, Apr. 2013.
[25] G. J. Byers and F. Takawira, "Spatially and temporally correlated MIMO channels: Modeling and capacity analysis," *IEEE Trans. Veh. Technol.*, vol. 53, no. 3, pp. 634–643, May 2004.
[26] A. Adhikary, J. Nam, J.-Y. Ahn, and G. Caire, "Joint spatial division and multiplexing—The large-scale array regime," *IEEE Trans. Inf. Theory*, vol. 59, no. 10, pp. 6441–6463, Oct. 2013.
[27] A. K. Jagannatham. (2016). *NOC: Estimation for Wireless Communications—MIMO/OFDM Cellular and Sensor Networks*. Accessed: Dec. 2, 2017. [Online]. Available: http://nptel.ac.in/courses/117104118/
[28] S. M. Kay, *Fundamentals of Statistical Signal Processing: Estimation Theory*. Englewood Cliffs, NJ, USA: Prentice-Hall, 1993.
[29] H. Yin, D. Gesbert, M. Filippou, and Y. Liu, "A coordinated approach to channel estimation in large-scale multiple-antenna systems," *IEEE J. Sel. Areas Commun.*, vol. 31, no. 2, pp. 264–273, Mar. 2013.
[30] E. Björnson, J. Hoydis, and L. Sanguinett, "Massive MIMO networks: Spectral, energy, and hardware efficiency," *Found. Trends Signal Process.*, vol. 11, nos. 3–4, pp. 154–655, Nov. 2017.
[31] J. Evans and D. N. C. Tse, "Large system performance of linear multiuser receivers in multipath fading channels," *IEEE Trans. Inf. Theory*, vol. 46, no. 6, pp. 2059–2078, Sep. 2000.
[32] P. Zhao, M. Zhang, H. Yu, H. Luo, and W. Chen, "Robust beamforming design for sum secrecy rate optimization in MU-MISO networks," *IEEE Trans. Inf. Forensics Security*, vol. 10, no. 9, pp. 1812–1823, Sep. 2015.
[33] M. Alageli, A. Ikhlef, and J. Chambers, "Optimal transmit power minimization in secure MU-MISO SWIPT systems," in *Proc. IEEE Int. Conf. Ubiquitous Wireless Broadband (ICUWB)*, Salamanca, Spain, Sep. 2017, pp. 1–7.
[34] M. Grant and S. Boyd. (Apr. 2011). *CVX: MATLAB Software for Disciplined Convex Programming, Version 1.21*. [Online]. Available: cvxr.com/cvx
[35] K. Zu, R. C. de Lamare, and M. Haardt, "Generalized design of low-complexity block diagonalization type precoding algorithms for multiuser MIMO systems," *IEEE Trans. Commun.*, vol. 61, no. 10, pp. 4232–4242, Oct. 2013.
[36] M. Razaviyayn, "Successive convex approximation: Analysis and applications," Ph.D. dissertation, Dept. Elect. Eng., Univ. Minnesota, Minneapolis, MN, USA, 2014.
[37] R. Tütüncü, K. Toh, and M. Todd. (Aug. 2001). *SDPT3—A MATLAB Software Package for Semidefinite-Quadratic-Linear Programming, Version 3.0*. [Online]. Available: http://www.math.nus.edu.sg/mattohkc/sdpt3
[38] A. Ben-Tal and A. Nemirovski, *Lectures on Modern Convex Optimization: Analysis, Algorithms, and Engineering Applications*. Philadelphia, PA, USA: SIAM, Jan. 2001.
[39] Y. S. Cho, J. Kim, W. Y. Yang, and C. G. Kang, *MIMO-OFDM Wireless Communications With MATLAB*. Hoboken, NJ, USA: Wiley, 2010.
[40] T. Le, K. Mayaram, and T. Fiez, "Efficient far-field radio frequency energy harvesting for passively powered sensor networks," *IEEE J. Solid-State Circuits*, vol. 43, no. 5, pp. 1287–1302, May 2008.
[41] R. M. Gray, "Toeplitz and circulant matrices: A review," *Found. Trends Commun. Inf. Theory*, vol. 2, no. 3, pp. 155–239, 2006.
[42] F. Zhang and Q. Zhang, "Eigenvalue inequalities for matrix product," *IEEE Trans. Autom. Control*, vol. 51, no. 9, pp. 1506–1509, Sep. 2006.
[43] G. Van Kempen and L. Van Vliet, "Mean and variance of ratio estimators used in fluorescence ratio imaging," *Cytometry A*, vol. 39, no. 4, pp. 300–305, 2000.

Mahmoud Alageli received the B.Sc. degree (Hons.) in electrical and electronic engineering from the Engineering Academy Tajoura, Tripoli, Libya, in 1999, and the M.Eng. degree in communication and computer from the National University of Malaysia, Malaysia, in 2006. He is currently pursuing the Ph.D. degree with the Intelligent Sensing and Communications Group, Newcastle University, Newcastle upon Tyne, U.K. From 2007 to 2011, he was an Assistant Lecturer with the Engineering Academy Tajoura. From 2012 to 2013, he was a Lecturer with the Faculty of Engineering, Garaboulli, Elmergib University, Libya. His current research interests include energy harvesting communications, physical layer security, and massive MIMO. He was a recipient of the "The Bright Bestowal 2006" organized by the Center of Graduate Studies, National University of Malaysia.

Aissa Ikhlef (M'09–SM'17) was born in Constantine, Algeria. He received the B.S. degree in electrical engineering from the University of Constantine, Constantine, Algeria, in 2001, and the M.Sc. and Ph.D. degrees in electrical engineering from the University of Rennes 1, Rennes, France, in 2004 and 2008, respectively. From 2004 to 2008, he was with Supélec, France, where he received the Ph.D. degree. From 2007 to 2008, he was a Lecturer with the University of Rennes 1. From 2008 to 2010, he was a Post-Doctoral Fellow with the Communication and Remote Sensing Laboratory, Catholic University of Louvain, Louvain La Neuve, Belgium. He was a visiting Post-Doctoral Fellow with the University of British Columbia, Vancouver, BC, Canada, in 2009. From 2010 to 2013, he was with the Data Communications Group, University of British Columbia, as a Post-Doctoral Fellow. From 2013 to 2014, he was with Toshiba Research Europe Limited, Bristol, U.K., as a Senior Research Engineer. From 2014 to 2016, he was with the School of Electrical and Electronic Engineering, Newcastle University, Newcastle upon Tyne, U.K., as a Lecturer (Assistant Professor). Since 2016, he has been an Assistant Professor with the Department of Engineering, Durham University, Durham, U.K. His current research interests include machine learning, energy harvesting communications, physical layer security, and massive MIMO. He has served as an Editor for the IEEE COMMUNICATIONS LETTERS from 2014 to 2016.

Jonathon Chambers (S'83–M'90–SM'98–F'11) received the Ph.D. and D.Sc. degrees in signal processing from the Imperial College of Science, Technology and Medicine (Imperial College London), London, U.K., in 1990 and 2014, respectively. From 1991 to 1994, he was a Research Scientist with the Schlumberger Cambridge Research Center, Cambridge, U.K. In 1994, he returned to the Imperial College London as a Lecturer in signal processing, and was promoted to Reader (Associate Professor) in 1998. From 2001 to 2004, he was the Director of the Center for Digital Signal Processing, and a Professor of signal processing with the Division of Engineering, King's College London, where he is currently a Visiting Professor. From 2004 to 2007, he was a Cardiff Professorial Research Fellow with the School of Engineering, Cardiff University, Cardiff, U.K. From 2007 to 2014, he led the Advanced Signal Processing Group within the School of Electronic, Electrical and Systems Engineering, Loughborough University, where he is a Visiting Professor. From 2015 to 2017, he was with the School of Electrical and Electronic Engineering, Newcastle University, where he is currently a Visiting Professor. Since 2017, he has been with the School of Engineering, Newcastle University, where he was a Professor of signal and information processing and led the Intelligent Sensing and Communications Group. In 2017, he became the Head of the Engineering Department, University of Leicester. He is also an International Honorary Dean and a Guest Professor within the Department of Automation, Harbin Engineering University, China. He has advised over 80 researchers through to Ph.D. graduation and published over 500 conference proceedings and journal articles, many of which are in IEEE journals. His research interests include adaptive signal processing and machine learning and their application in communications, defense and navigation systems.

Dr. Chambers is a fellow of the Royal Academy of Engineering, U.K., the Institution of Engineering and Technology, and the Institute of Mathematics and its Applications. He has served on the IEEE Signal Processing Theory and Methods Technical Committee for six years, the Jack Kilby Medal Committee for three years, and the IEEE Signal Processing Society Awards Board for three years. He was the Technical Program Co-Chair for the 36th IEEE International Conference on Acoustics, Speech, and Signal Processing (ICASSP), Prague, Czech Republic, and is serving on the organizing committees of the ICASSP 2019 Brighton, U.K., and the ICASSP 2022, Singapore. He has also served as an Associate Editor for the IEEE TRANSACTIONS ON SIGNAL PROCESSING for three terms over the periods of (1997–1999) and (2004–2007). He was a Senior Area Editor from 2011 to 2015.